Seafloor spreading event in western Gulf of Aden during the November 2010-March 2011 period captured by regional seismic

Geophysical Journal International

Geophys. J. Int. (2016) **205,** 1244–1266
Advance Access publication 2016 February 22
GJI Geodynamics and tectonics

doi: 10.1093/gji/ggw068

Seafloor spreading event in western Gulf of Aden during the November 2010–March 2011 period captured by regional seismic networks: evidence for diking events and interactions with a nascent transform zone

Abdulhakim Ahmed,[1,2,3] Cécile Doubre,[4] Sylvie Leroy,[2,3] Mohamed Kassim,[5,†] Derek Keir,[6] Ahmadine Abayazid,[5] Perrot Julie,[7] Audin Laurence,[8] Jérome Vergne,[4] Nercessian Alexandre,[9] Eric Jacques,[9] Khaled Khanbari,[10] Jamal Sholan,[1] Frédérique Rolandone[2,3] and Ismael Al-Ganad[11]

[1]*Seismological and Volcanological Observatory Center, Herran Garden,* 82187 *Dhamar, Yemen. E-mail: hakim66@myself.com*
[2]*Sorbonne Universités, UPMC Univ Paris* 06, *UMR* 7193, *Institut des Sciences de la Terre Paris (iSTeP), F-*75005 *Paris, France*
[3]*CNRS, UMR* 7193, *Institut des Sciences de la Terre Paris (iSTeP), F-*75005 *Paris, France*
[4]*Institut de Physique du Globe de Strasbourg, UMR* 7516, *Université de Strasbourg/EOST, CNRS,* 5 *rue René Descartes, F-*67084 *Strasbourg Cedex, France*
[5]*The Arta Geophysical Observatory, Arta, Djibouti*
[6]*National Oceanography Centre Southampton, University of Southampton, Southampton SO*14 3*ZH, UK*
[7]*Domaines Océaniques, IUEM, CNRS, Place Nicolas Copernic, F-*29280 *Plouzané, France*
[8]*Institut de Recherche pour le Développement, ISTERRE, Grenoble, France*
[9]*Institut de Physique du Globe de Paris; UMR* 7154, 1 *rue Jussieu, F-*75252 *Paris, France*
[10]*Department of Environmental and Earth Sciences, Sana'a University, Sana'a, Yemen*
[11]*Yemen Geological Survey & Mineral Resources Board, Sana'a, Yemen*

Accepted 2016 February 15. Received 2016 February 15; in original form 2014 December 6

SUMMARY

In November 2010, intense seismic activity including 29 events with a magnitude above 5.0, started in the western part of the Gulf of Aden, where the structure of the oceanic spreading ridge is characterized by a series of N115°-trending slow-spreading segments set within an EW-trending rift. Using signals recorded by permanent and temporary networks in Djibouti and Yemen, we located 1122 earthquakes, with a magnitude ranging from 2.1 to 5.6 from 2010 November 1 to 2011 March 31. By looking in detail at the space–time distribution of the overall seismicity, and both the frequency and the moment tensor of large earthquakes, we re-examine the chronology of this episode. In addition, we also interpret the origin of the activity using high-resolution bathymetric data, as well as from observations of seafloor cable damage caused by high temperatures and lava flows. The analysis allows us to identify distinct active areas. First, we interpret that this episode is mainly related to a diking event along a specific ridge segment, located at E044°. In light of previous diking episodes in nearby subaerial rift segments, for which field constraints and both seismic and geodetic data exist, we interpret the space–time evolution of the seismicity of the first few days. Migration of earthquakes suggests initial magma ascent below the segment centre. This is followed by a southeastward dike propagation below the rift immediately followed by a northwestward dike propagation below the rift ending below the northern ridge wall. The cumulative seismic moment associated with this sequence reaches 9.1×10^{17} Nm, and taking into account a very low seismic versus geodetic moment, we estimate a horizontal opening of ∼0.58–2.9 m. The seismic activity that followed occurred through several bursts of earthquakes aligned along the segment axis, which are interpreted as short dike intrusions implying fast replenishment

†Deceased.

of the crustal magma reservoir feeding the dikes. Over the whole period, the opening is estimated to be ∼1.76–8.8 m across the segment. A striking feature of this episode is that the seismicity remained confined within one individual segment, whereas the adjacent en-echelon segments were totally quiescent, suggesting that the magma supply system of one segment is disconnected from those of the neighbouring segments. Second, we identify activity induced by the first intrusion with epicentres aligned along an N035°E-trending, ∼30 km long at the northwestern end of the active opening segment. This group encompasses more than seven earthquakes with magnitude larger than 5.0, and with strike-slip focal mechanisms consistent with the faults identified in the bathymetry and the structural pattern of the area. We propose that a transform fault is currently in formation which indicates an early stage of the ridge segmentation, at the locus of the trend change of the spreading ridge, which also corresponds to the boundary between a clear oceanic lithosphere and the zone of transform between continental and oceanic crust.

Key words: Earthquake source observations; Seismicity and tectonics; Mid-ocean ridge processes; Transform faults; Submarine tectonics and volcanism; Dynamics: seismotectonics.

1 INTRODUCTION

1.1 Rifting episodes on the Aden/Red-Sea area

During the last decade, several important seismovolcanic events have occurred in Afar and its surrounding areas of the Red Sea and the Western Gulf of Aden (Fig. 1a), confirming the importance of volcanism in this extensional region above an abnormally warm mantle (Rooney *et al*. 2012; Ferguson *et al*. 2013; Hansen & Nyblade 2013). Since most of the events affected subaerial volcano-tectonic segments, they offered an opportunity to study the tectonic deformation and the magmatotectonic interactions involved in the active rifting process using the combination of geodetic techniques and seismology. In the Afar Depression, the so-called «Ardukoba» event in the Asal-Ghoubbet rift segment (Djibouti) in 1978, one of the first seismovolcanic events to have been monitored with geophysical methods, shed light on the important role of dike intrusions on the observed surface deformation (Abdallah *et al*. 1979). More recently, 14 dike intrusions have been identified along the ∼60 km long Dabbahu–Manda-Hararo (D-MH) rift segment between 2005 and 2010 from InSAR data (Wright *et al*. 2006; Grandin *et al*. 2009, 2010; Hamling *et al*. 2009) and accompanied with hour to day long seismic swarms (Ebinger *et al*. 2008; Ayele *et al*. 2009; Keir *et al*. 2009; Grandin *et al*. 2010; Belachew *et al*. 2011; Grandin *et al*. 2011). Other signs of volcanic activity have been observed in southern Afar with the 2000 intrusion near the Ayelu-Amoissa volcanic chain (Keir *et al*. 2011). In northern Afar, Alu-Dalafilla erupted in November 2008 and was associated with sill deflation and dike intrusion (Pagli *et al*. 2012), and in November 2010 Erta Ale lava lake rose to over-spill the inner crater (Field *et al*. 2012). The most recent documented magmatic event is the June 2011 eruption and subsidence of Nabro volcano (Ebinger *et al*. 2013; Hamlyn *et al*. 2014). Previous to these events, a dike intrusion and induced fault slip were observed near Dallol in October 2004 (Nobile *et al*. 2012). Further east, along the Sheba ridge and offshore Oman, volcanic activity is reported (Lucazeau *et al*. 2009; d'Acremont *et al*. 2010; Leroy *et al*. 2010a). Further north, in NW Saudi Arabia, May 2009 marks a new episode of seismic activity in the Harrat-Lunayyir volcanic field (Al-Amri *et al*. 2012; Al-Zahrani *et al*. 2012), where InSAR data helped to constrain this episode as a dike intrusion (Baer & Hamiel 2010; Pallister *et al*. 2010).

In agreement with previous studies of similar events in oceanic domain (e.g. Sigurdsson 1980), the displacement measurement associated with most of these seismovolcanic events, when they exist, are consistent with a horizontal opening across the rift, a narrow elongated subsidence zone along the rift inner floor, uplift of the margins and a local subsiding area below the main volcanic centre (Rubin & Pollard 1988). Together with the seismic data showing a lateral migration of the earthquakes (Brandsdöttir & Einarsson 1979), they confirm that dike intrusions accommodate significant deformation over short time-scales and that dikes are fed by sometimes complex crustal magma plumbing systems (Wright 2012). A less well-constrained magmatic event in the Red Sea is the relatively aseismic eruptions starting September 2007 at Jebel-Attair Island ending longer than a century of quiescence. In November 2011, NASA reported this activity caused birth of a volcanic island at Al-Zubair archipelago. Due to most activity occurring below the sea surface deformation could not be seen.

Along submarine mid-oceanic ridges, the monitoring of active rifting process is usually achieved through seismic data from local or regional oceanic ocean bottom seismometer and autonomous underwater hydrophone networks (Fox *et al*. 1995; Blackman *et al*. 2000; Dziak *et al*. 2009) or global land-based instruments (e.g. Tolstoy *et al*. 2001, 2009). These seismic surveys reveal important oceanic spreading-related processes including the migration of the seismic activity (Fox *et al*. 1995), the role of fluids, and the slip activation on normal or transform faults in response to probable magmatic emplacements (Tolstoy *et al*. 2001; Dziak *et al*. 2009).

In this paper, we present the results from a regional seismic survey of the November 2010 episode along the oceanic ridge in the western Gulf of Aden. In doing so we improve significantly the precision in earthquake location, moment tensor inversion and magnitude cut-off of earthquakes achieved from global records (Shuler & Nettles 2012). We interpret our results in light of the recent seismic and geodetic observations made in the region along subaerial segments in order to better understand opening dynamics of the spreading segment and its relationship with fault activity. In addition, we use the high-precision earthquake locations along with high-resolution bathymetry data to discriminate between dike-induced faulting near the dike and later induced slip on a nearby transform fault.

1.2 Geodynamical setting

The Gulf of Aden rifted margins transition from being volcanic in the west, to non-volcanic or including little evidence of magmatism in the east (Ahmed *et al*. 2014; Corbeau *et al*. 2014; Korostelev *et al*. 2014). The Gulf of Aden can be divided into three main parts based on sedimentation and structural styles (Autin *et al*. 2010a; Leroy *et al*. 2012; Bellahsen *et al*. 2013). With an extension direction of N020°E, the eastern part is characterized by continuous calcareous sedimentation since the onset of the rifting (east of Alula-Fartak Fracture zone, AFFZ; Leroy *et al*. 2012; Robinet *et al*. 2013). The central part, between the AFFZ and Shukra-el-Sheik fracture zones (SSFZ), shows uplift and erosion with a subaerial to shallow sedimentation during the rifting (mudstones, evaporites and reefal limestones; Leroy *et al*. 2012). West of SSFZ, the western part of the Gulf, has been under the influence of Afar plume with a variable spreading ridge trend and extension direction (Tard *et al*. 1991; Hébert *et al*. 2001; Leroy *et al*. 2010a). The slow-spreading rate along the Aden and Sheba Ridges progressively increases from west to east from 1.6 cm yr^{-1} at the entrance of the Gulf of Tadjura to 2.4 cm yr^{-1} at the Aden-Owen-Carlsberg triple junction (Fig. 1a; Fournier *et al*. 2001, 2010).

The westernmost part of the Aden Ridge presents a straight ridge with no first-order segmentation whereas the central part is more segmented with seven transform faults that offset the ridge in a left-stepping fashion by successive transforms ranging from 14 to 47 km (Fig. 1). Detailed studies of the eastern part of the Gulf of Aden demonstrate that between the long-lived AFFZ and Socotra Hadbeen fracture zone (SHFZ; Fig. 1a) the oceanic ridge segmentation changes from three to two segments. Changes in volcanic feeding of the oceanic ridge and plate kinematics are proposed (d'Acremont *et al*. 2006, 2010).

Within the westernmost part of the Gulf of Aden, where the spreading ridge is linear, three distinct lithospheric domains are again identified based on gravity data (Hébert *et al*. 2001) and magnetic data (Leroy *et al*. 2012; Fig. 1b). The well-developed eastern domain, which lies between E044.30° and E045° (Fig. 1b), is characterized by an 8 km thick oceanic crust on either side of the ridge (Hébert *et al*. 2001) with magnetic anomalies defined as chron A5

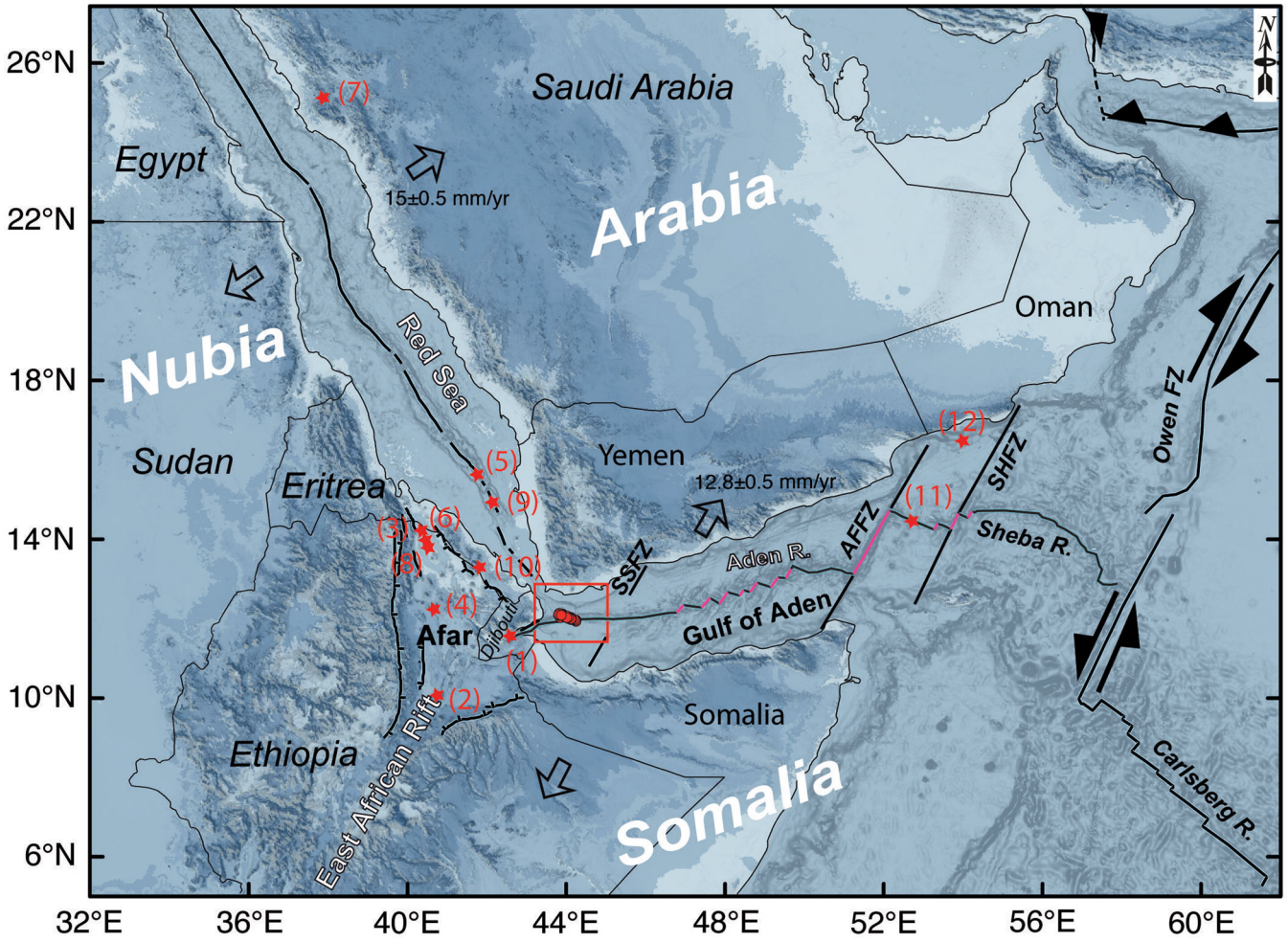

Figure 1. (a) Geodynamical context of Arabia, Nubia and Somalia plates, with the locations of the known volcanotectonic episodes [1—Asal-Ghoubbet rift segment (1978); 2—Ayalu-Amoussia (2000); 3—Dallol (2004); 4—Manda-Harraro–Dabbahu segment (2005–2010); 5—Jebel Ait Tair (2007); 6–Alu-Dallafila (2008); 7—Harrat-Lunayyir (2009); 8—Erta Ale eruption (2010); 9—Al Zubair (2011); 10—Nabro (2011); 11—Sheba ridge; 12—offshore Oman; see references in the text]. SSFZ: Shukra El-Sheik fracture zone; AFFZ: Alula Fartak fracture zone; SHFZ: Socotra Hadbeen Fracture zone. The transform faults are drawn in pink. Relative plate velocities in the region are given by DeMets *et al*. (2010). (b) Morphotectonic features along the western part of the Aden ridge, the location indicated by red rectangular in panel (a), modified from Audin (1999). Magnetic anomalies and structural features are from Leroy *et al*. (2012).

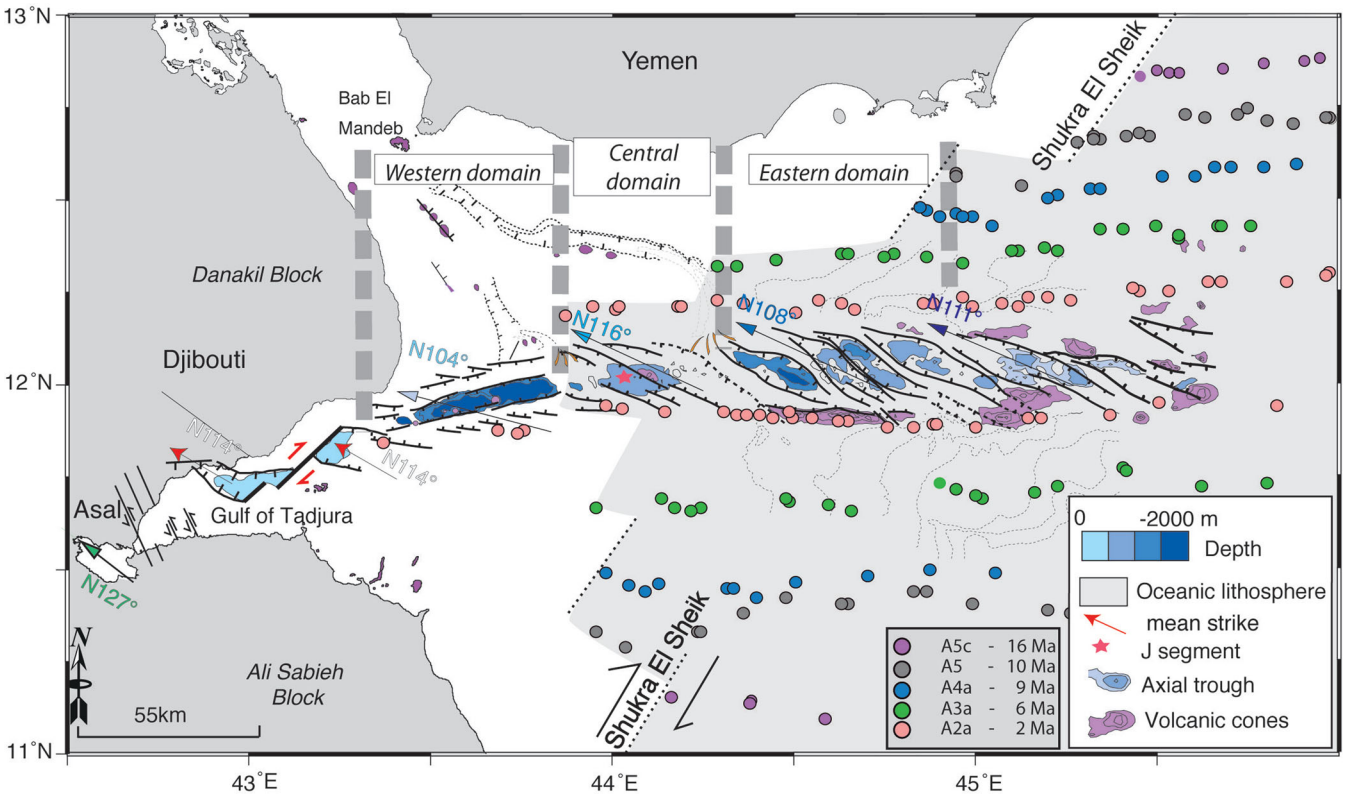

Figure 1. (*Continued*).

(10 Ma) at the eastern part of the domain and A3a (6 Ma) at the western part of the domain (Tard *et al*. 1991; Audin 1999; Dauteuil *et al*. 2001; Hébert *et al*. 2001; Leroy *et al*. 2012). The central domain, located at E043.90° to E044.30° (Fig. 1b), marks the lithospheric transform between the well-developed oceanic lithosphere to a transitional lithosphere toward the African continent with the magnetic anomaly corresponding to chron A2a (2 Ma) on both sides of the spreading axis (Leroy *et al*. 2012). The crustal thickness of this domain is approximately 9–12 km below the ridge (Laughton *et al*. 1970; Hébert *et al*. 2001). Recent volcanic activity has been identified in this domain where most of the axial valley is covered with recent lava flows (Dauteuil *et al*. 2001). The western domain is located from E043.90° to the entrance of the Gulf of Tadjura, and has a spreading ridge with a trend ranging from EW to ∼N075°E with a 10–15 km wide axial valley. Four important basins, with two of them being the deepest basins west of Shukra El-Sheik fracture zone (SSTF), are 1650 m deep (Dauteuil *et al*. 2001). No oceanic crust has been clearly identified for this domain (Dauteuil *et al*. 2001), although the magnetic anomaly chron A2a (2 Ma) is observed on the southern shoulder of the spreading axis as well as the axial magnetic anomaly (Leroy *et al*. 2012; Fig. 1b). Courtillot *et al*. (1980) proposed the existence of an incipient oceanic crust within the Gulf of Tadjura and the subaerial domain in Djibouti from aeromagnetic data. In contrast, Hébert *et al*. (2001) suggested stretched and thinned continental crust of 15–20 km thick computed from gravity data. From oceanic magnetic anomalies identification and the bathymetric data, the Aden spreading ridge shows numerous clear volcanic edifices and cones providing evidence for magma involvement in the rifting process (Leroy *et al*. 2010a).

2 DATA AND METHODS

2.1 Location process and velocity

We combined the data recorded by both permanent and temporary seismic networks in Djibouti and Yemen presented in Fig. 2 and in Aux_Mat-1 (Supporting Information). Both temporary networks were fully completed by 2010 December 15.

The determination of the velocity structure in the region is complex because of three main reasons: (1) the main active area is located along the ridge axis where oceanic spreading potentially occurs; (2) the stations in Yemen are located on the continental plateau; and finally (3) because the structure in Afar, and more specifically in Djibouti, is still debated between an oceanic crust (Ruegg 1975; Barberi *et al*. 1980), a continental crust (Makris & Grinzburg 1987) and a continental crust intruded by gabbroic and granitic plutons (Mohr 1987). Several distinct velocity models derived from active seismic profiles exist, and are presented in Aux_Mat-2 (Supporting Information). All the models are characterized by a thin crust. Following Laughton & Tramontini (1969), this area is also characterized by an abnormal upper mantle velocity structure with a velocity (7.1 km s^{-1}) lower than typical mantle velocity range (>7.8 km s^{-1}). Similar results have been reported by Ruegg (1975) within the Gulf of Tadjura west of the activity area, with anomalous mantle velocities (6.7–6.9 km s^{-1}). We then tested ten different crustal and upper mantle velocity models and the final model was selected using the criteria of minimum station residuals and minimum root mean square (rms) for the location of the 50 events encompassing at least 25 arrival times. We used a fixed Vp/Vs of 1.78 (Ahmed *et al*. 2013).

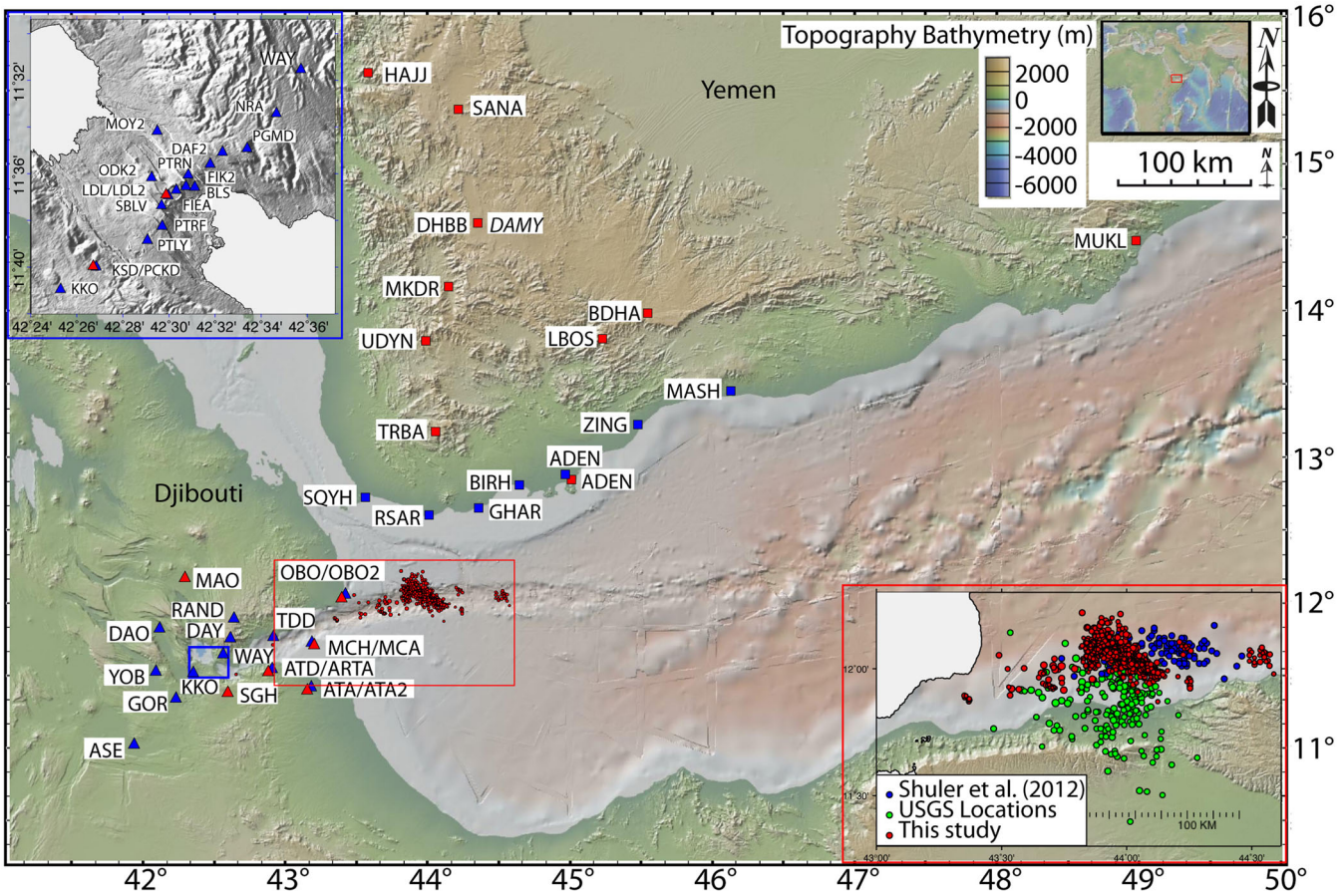

Figure 2. Seismic networks during the period under study. The triangles and squares show the locations of the stations in Djibouti and Yemen, respectively. The red and blue symbols correspond to the permanent and temporary stations, respectively. The locations of the 1122 events located in this study have been indicated by red circles. The insert at the top left corner is a zoom of the network in the centre of the Asal-Ghoubbet Rift. The insert at the bottom right corner is the seismicity recorded between 2010 November 10 and 2011 March 31. The blue and green dots are the events located by Shuler & Nettles (2012), by USGS, respectively. The locations determined in this study correspond to the red dots.

We analysed the seismic activity, from 2010 November 1 to 2011 March 31, during which several thousand of events were recorded. Using the selection criterion of picking at least a *P*-phase at seven stations and *S*-phase at two stations, 1400 events were selected for further analysis. A total of 21 649 *P*-wave arrival times were manually picked on the vertical component and 7202 *S*-wave arrival times were picked on horizontal components for three-channel stations and on vertical for single channel stations. The location process of some events has been difficult because most of the events have small amplitude emergent body-wave arrivals and because signals of distinct events are overlapping due to the intense seismic activity especially at the beginning of the period. Finally, we located a final set of 1122 regional earthquakes using the SEISAN software package (Ottemöller *et al*. 2011). In the final set, every earthquake has an average rms (root mean square of traveltime residuals) lower than 0.4 s. With the exception of 8 events, the horizontal and vertical errors are less than 3.75 and 5.0 km and below 2.0 and 2.5 km because of the network evolution on December 15, respectively (Aux_Mat-3, Supporting Information). The complete network allows a wide cover of azimuths. Therefore, the values of the horizontal errors for the locations deduced from this regional network are significantly lower than the lateral location uncertainties given from centroid moment determinations which are between 1 and 13 km (Shuler & Nettles 2012).

The local magnitude of our set of localized seismic events ranges from 2.1 to 5.6.

2.2 Moment tensor inversion

We performed a moment tensor inversion to estimate the source parameters (seismic moment, moment magnitude and fault type) of strong and moderate earthquakes ($M_L \geq 4.0$) recorded by our seismic networks (Dziewonski *et al*. 1981; Kikuchi & Kanamori 1991; Dreger & Helmberger 1993; Kawakatsu 1995). Using Moment Tensor Inversion program from regional networks coded by Yagi (2004), we analysed the three-component seismograms recorded at broadband stations for events with M_L above 4.0. Because of the network configuration, we chose to not take into account the isotropic component. The observed data were windowed 5 s before and 80 s after the *P* phase arrival time, then filtered from 11 to 25 s. Since we previously located events using a dense regional seismic network, we only explored the effect of centroid depths on the results of the moment tensor solution. Therefore to test the focal depth of the event determined by the location program and the stability of the used velocity model employed, we changed the depths of the hypocentre and selected the depth corresponding to the minimal variance. We estimated the depth accuracy of about ±1–2 km.

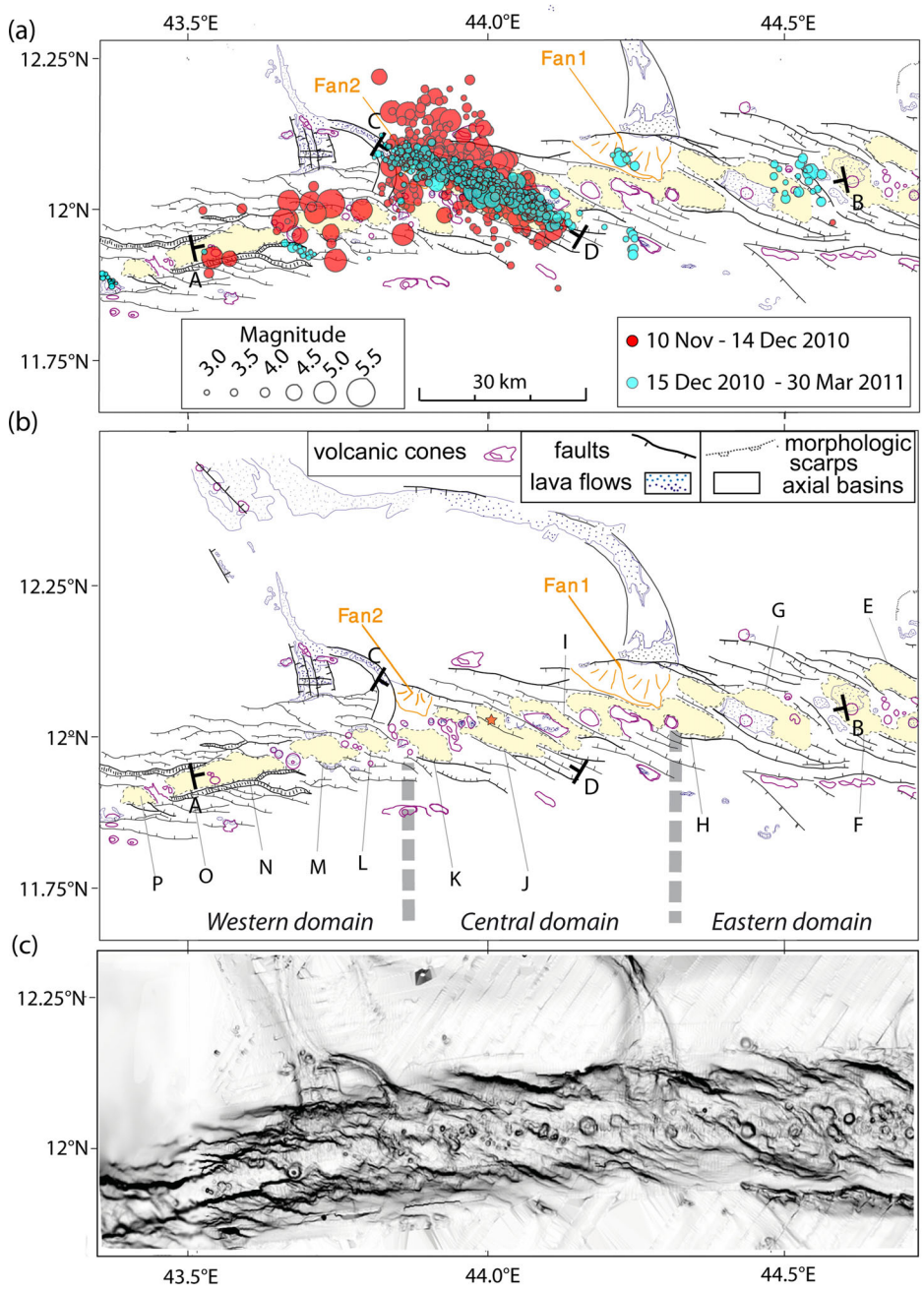

Figure 3. (a) Seismicity recorded from 2010 November 10 to 2011 March 30. (b) Morphotectonic features from Audin (1999); location in Fig. 1. The orange star indicates the location of the melted optical wire and hot surface sea water observations (see Section 6). (c) Shaded bathymetric data of the area under study.

In order to estimate the seismic energy released during the period of activity, we establish the linear fit between the local magnitude (M_L) and the logarithm of the seismic moment from the set of events for which we estimated the moment tensor (Aux_Mat-4, Supporting Information).

3 MAIN ACTIVITY

3.1 Spatial distribution and main tectonic/volcanic features

During the analysed time period, the seismic activity in this area is high, with up to 73 located events d^{-1} on 2010 November 14. From November 2010 to the end of March 2011, the activity is characterized by high-magnitude events, including 29 with $M_L \geq 5.0$, and a maximum recorded magnitude of 5.6. The activity is characterized by small isolated clusters located between (043.5°E, 11.80°N) and (044.6°E, 12.25°N), that is, within a 120 km EW-long and 40 km NS-wide rectangular area (Fig. 3a). More than 95 per cent of the located events are concentrated within the ridge valley. Below, we refer to segments (E–O) and canyons (1, 2) following the naming given by Audin (1999) from bathymetric and reflectivity data acquired during the Tadjouraden cruise in 1995 (Audin 1999; Dauteuil *et al*. 2001; Figs 3b and c).

The area affected by this intense seismic activity is located in the western part of the central domain (Section 1.2, Figs 1b and 3a) within the ∼20 km wide axial valley. Four en-echelon N115°

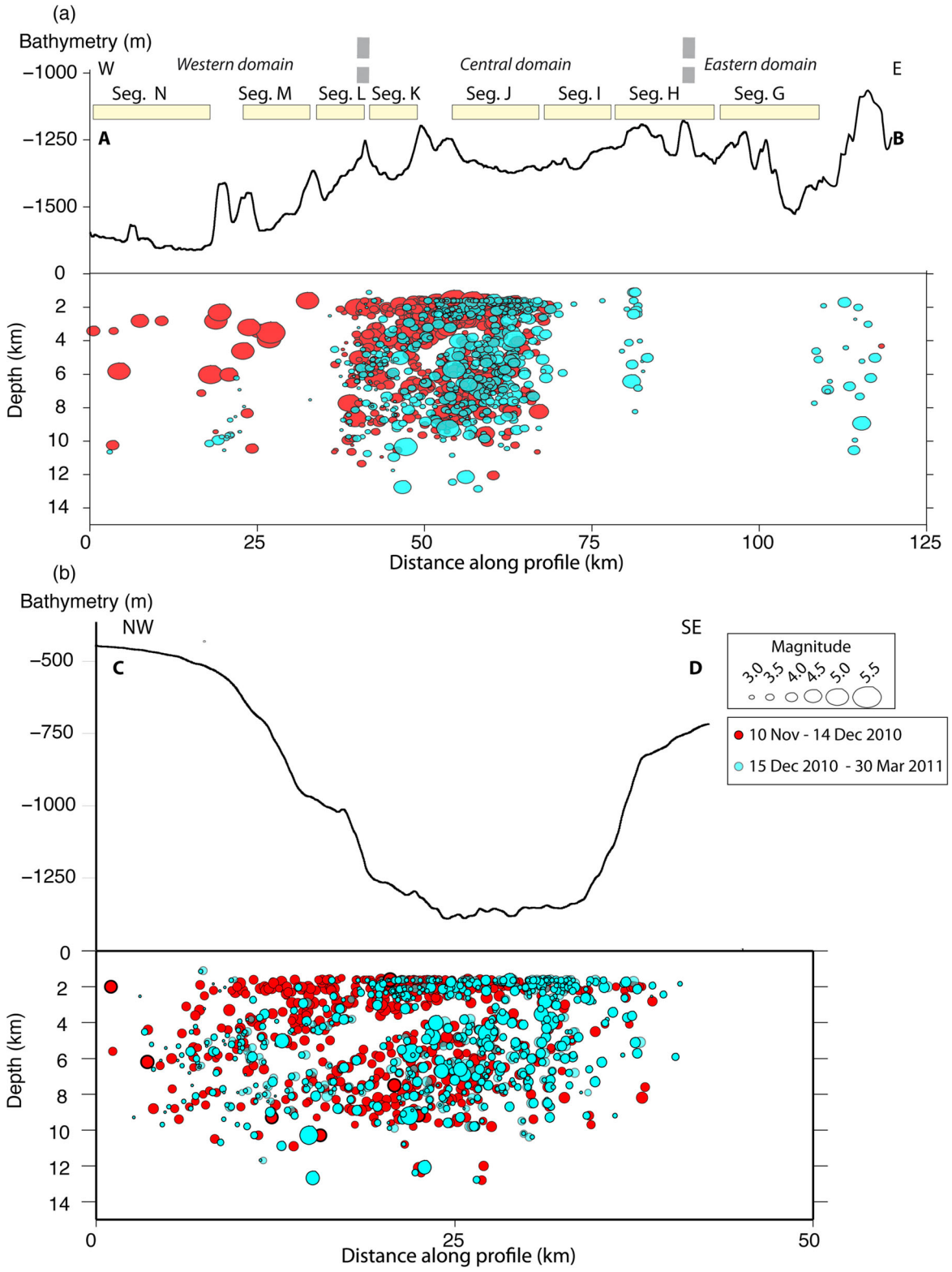

Figure 4. Hypocentre and bathymetry cross-sections, locations indicated in Fig. 3(a). (a) EW-trending cross-section along the ridge (b) NW–SE-trending cross-section along the segment J axis. The horizontal scale is not the same for the two profiles. The arrows on the profile (b) indicate the area of low superficial activity.

E-trending basins dissect the axial valley formed by N100°E- to N140°E-trending, ∼20 km long and ∼100 m high normal faults. The depth of the axial valley ranges from 1000 to 1500 m with the most superficial part corresponding to the central graben of segment J (Figs 1b and 4a). Near segment J, the vertical throw of the main normal faults bounding the ridge valley ranges from 300 to 500 m and decreases eastwards (Fig. 4b). On the northern ridge margin, two ∼300 m deep, 1–6 km wide, ∼NS-trending canyons run from

the southern Red Sea through the Bab El Mandab strait, to the axial valley and end by forming large fans along the northern ridge wall (fan 1 and fan 2; Audin 1999; Dauteuil *et al*. 2001). At the southern end of the western canyon, a NS-trending graben is bounded by four ∼N170°E-striking normal faults. This graben is restricted in the north by chains of volcanic cones, and two EW-striking large faults in the south. Also, a narrow EW-trending graben intercepts this graben at right angles in its central part (Figs 3b and c). The large deposits of fan 2 have been shifted to the east and the canyon channel flows through a curved channel to the east of the graben, cutting the western side of the fan deposits and running southwestwards down to the inner-floor of segment L. The relative location of the eastern canyon and its associated fan 1 implies a right-lateral strike-slip movement along the E–W bounding normal fault. Assuming extension directed N037°E, Dauteuil *et al*. (2001) ascribed a 5 km shift with a spreading rate of 2 cm yr^{-1} since 300 ky. Oblique normal faults with a right-lateral strike-slip component are observed in this domain of the Aden Ridge, consistent with the NW–SE-trending faults and the left-stepping en-echelon pattern with respect to the valley E-W-trending walls (Dauteuil *et al*. 2001).

The spatial distribution of the seismic activity clearly shows a main swarm centred at E044.000°-N12.042° (Fig. 3a). It includes 1032 earthquakes with magnitude ranging from 2.2 to 5.5, consisting of 90 per cent of the total number of events. The shape of the main N115°E-trending and 40 km long swarm reveals that the episode is mainly related to the activity of one individual spreading segment, segment J, located east of the fan 2. Segment J extends from the southern ridge wall, characterized by short en-echelon NW–SE normal faults, to the northern ridge wall of the main axial valley. Near the segment centre and at the NW end of the central graben of the segment, at the base of northern ridge wall, chains of volcanic cones with a mean trend of N115°E-N130°E are aligned parallel to the bounding faults (Figs 3b and c). The majority of the epicentres (∼700 events) lie within the deep central graben formed by antithetic NW-trending normal faults. We note that the adjacent en-echelon segments K and I are completely inactive during this period.

Thirty kilometres west of the main swarm, a cluster of 39 moderate size seismic events was detected. Near segments M and N, strong events, eight of which have magnitude above 5.0, occurred along the northern and southern walls of the main valley as well as on the N130°E-trending transverse ridge which is made of volcanic cones, recent basaltic flows and normal faults (Choukroune *et al*. 1988; Figs 3 and 4a). This area is characterized by steep E–W-trending normal faults forming most of the bathymetry along the northern and southern walls. More recent and smaller N130°E-trending normal faults cut the ridge walls resulting to an en-echelon structure of the ridge wall. At this longitude, the cumulative height of the ridge walls exceeds 1600 m.

In addition, three small seismic clusters, encompassing ∼51 events, with magnitude below 4.7, occurred during the study at different locations along the ridge: longitude E043.36°, E044.23° and E044.52° (Fig. 4). In agreement with the time-space analysis below, we do not consider these clusters to be directly related to the main activity of the episode. The westernmost cluster at E043.36° occurred offshore within the Gulf of Tadjura, south of the city of Obock, near a volcanic cone located southwest of segment P (Figs 2 and 3). The events of the cluster at E044.23° are aligned along the scarp resulting from the overlap of two deposit cones forming the fan 1 (Fig. 3). Finally, the cluster at E044.52° is located between segments G and F, where the seafloor is structured by volcanic cones and ∼N135°E-trending, SW-dipping normal faults (Fig. 3).

As shown in Fig. 2, the epicentres of the events recorded during this period and located by the NEIC agency are shifted to the south relative to our locations by 0.2°. In contrast, the epicentre locations of Shuler & Nettles (2012) are shifted to the east by 0.2° with respect to our results. Their locations of the main activity are centred at (E044.22°, N12.07°), that is, at the base of fan 1 coming out of the eastern canyon, and they extend along the NW direction towards the northern ridge wall, north of segment I (Fig. 3). The seismicity of the westernmost cluster is more diffuse than the distribution we achieve since the epicentres are distributed from the northern wall to the southern wall of the ridge, west of segment J. Therefore, segment J appears aseismic according to the locations determined by Shuler & Nettles (2012), while it corresponds to the main active area in our analysis. The difference of epicentral locations between global determinations [Preliminary Determination of Epicentres (PDE) from United States Geological Survey (USGS)] and regional inversion are expected to be due to the difference of spatial cover of the monitoring network. In the case of the USGS locations (first arrival times), the heterogeneity of the stations explains the shift with our locations from the regional network. In the case of the centroid moment tensor (CMT) catalogue, the lateral (and vertical) shift results primarily from the Earth three-dimensional structure used for the inversion algorithm, which does not take into account lateral heterogeneity, as showed for instance by Hjörleifsdottir & Ekström (2010).

3.2 Depth distribution

Due to both the distribution of our seismic stations at the time of the swarm onset and the distance between the stations and the active area (∼80 km), any analysis of the hypocentre depth has to be done with caution. However, as we mentioned in Section 2.1, the network configuration was enhanced within the first month giving a better accuracy on the depth determination. The focal depths of the main swarm range from 1.6 to 12.8 km, which is consistent with other slow-spreading oceanic ridge segments (Toomey *et al*. 1985; Huang & Solomon 1988; Wolfe *et al*. 1995; Cannat 1996; Fig. 4). A large number of events are located at a shallow depth less than 2 km, especially at the central part of the segment J. The seismic activity is deeper, up to ∼10.0 km depth (Fig. 4b). We note however some alignments at the depth levels of 1.6, 2.0 and 2.1 km below the central graben probably resulting from the discontinuity of our crustal velocity model at 2.0 km. These alignments disappear at the SE and NW ends of the segment J where one notable feature is the ∼15°-dipping ∼2.5 km thick gap of seismicity extending from 10.0 km depth below the northern margin to the area at 3.5 km depth below the central graben (Figs 4a and b). It is compelling to note that this gap of seismic activity and its shape appear early during the episode and does not evolve over the whole period of monitoring.

4 SOURCE MECHANISMS AND FREQUENCY CONTENT

4.1 Focal mechanisms

Due to the strict selection criteria we adopted, the close occurrence of events in time and the relatively short hypocentre-station distance, several events with P onset in the coda of previous events have not been located. This reduces the total number of moment tensor solutions to 99 events compared to the 110 events CMT solutions determined by Shuler & Nettles (2012), who used teleseismic data

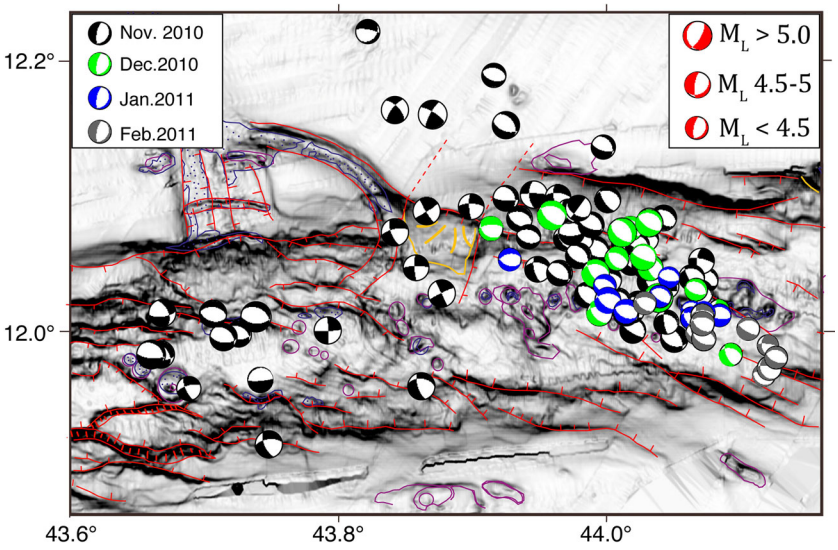

Figure 5. Focal mechanisms determined over the November 2010–March 2011 period.

recorded by remote seismic stations (epicentral distance >670 km) over a six-month period from November 2010 to April 2011.

In our analysis, 78 per cent of the solved 99 events occur within segment J and the remainder belong either to the high-magnitude western cluster or to the transfer zone between the central and western domains (Fig. 5). We distinguish three categories. First, 60 per cent of the earthquakes are characterized by normal faulting with a major trend of NW–SE. Second, 20 per cent of the earthquakes are characterized by normal faulting with a right-lateral strike-slip component. Third, 17 per cent of the earthquakes are characterized by strike-slip mechanism, including 11 per cent with pure strike-slip movement and 6 per cent with a slight component of normal faulting. We note only one event with left-lateral strike-slip faulting and two events with a reverse mechanism. The fault mechanism patterns are discussed in the following section.

Overall, our fault plane solution and the CMT solutions (Shuler & Nettles 2012) are very similar. The discrepancies are mainly due to the location differences of the hypocentres. Unlike Shuler & Nettles (2012), we do not constrain the hypocentral depth to 12 km, since it would be larger than the ∼10 km thick crust according to the seismic data in the western Gulf of Aden (Laughton & Tramontini 1969) and more generally according to the knowledge of the crustal structure along the spreading axis of mid-oceanic ridges (Cannat 1996) and its seismogenic behaviour (Weidner & Aki 1973; Toomey *et al.* 1985).

Our focal mechanism solutions are consistent with the structures inferred from the bathymetry and/or seismic profiles (Manighetti *et al.* 1997; Audin 1999; Dauteuil *et al.* 2001). First, the seismic activity concentrated within the inner floor of segment J is largely dominated by normal faulting mechanisms along N100°E- to N140°E-trending planes. This corresponds to the mean direction of the normal faults and the alignments of volcanic cones. We note that the mechanisms showing strike-slip faulting or normal faulting with a significant strike-slip component are located on the edges of segment J, at its two northwestern and southeastern ends and on its eastern border. This probably results from the complex structure of the ridge valley at this part of the Aden ridge, where the opening segments are perpendicular to the extension direction and the ridge walls are oblique to the N037°E-trending extension direction, inducing lateral slip on E–W-trending normal faults. At the NW end of segment J, several types of focal mechanisms exist, consistent with the two sets of normal faults (NW–SE-trending and E–W-trending) and strike-slip faulting along the EW-trending direction (Fig. 5). Moreover, the complexity of the transform zone between the central and western domains is shown by three sets of strike-slip mechanisms with normal component for some of them and whose nodal planes are parallel to the following trends: N087° ± 10°E/N177° ± 10°E, N039° ± 8°E/N129° ± 8°E and N065° ± 8°E/N155° ± 8°E (Fig. 5). From bathymetry data and the seismicity, it is clear that there is a transform area between the central and western domains, since all the structural features from the east and west end at this level of the ridge and where both left and right strike-slip movement occur (e.g. Shuler & Nettles 2012).

Finally, at the westernmost area of the activity, the mechanisms are consistent with a dominant ∼N100°-trending normal faulting for the events located along bounding faults of segments M and L. We note also that the events located on or near the southern wall are characterized by strike-slip faulting with a normal component, consistent with right-lateral slip on the N080°-trending normal faults (Fig. 5).

4.2 Frequency content

Our seismic stations are more than ∼80 km from the source area, and as such the frequency content of the seismograms is likely influenced by path effects including attenuation. We therefore interpret our waveforms and spectra with caution. However, because all the events are located within a small area and therefore affected by the same path effect, we compare arrivals from different earthquakes at similar stations to identify distinct earthquake types. The first group of earthquakes is characterized by emergent low amplitude body waves with the whole spectrum below 2 Hz for all stations, implying that the LF content is neither due to the path nor to the site effects, but related to the source. An example of this kind of low-frequency (LF) earthquake recorded at the station OBO2 in Obock in Djibouti is shown in Fig. 6(a). We observe a dominant frequency at ∼0.5 Hz (see signals and spectrograms at three other stations in Aux_Mat-3, Supporting Information). Another characteristic of the LF earthquakes is the long coda, which lasts more than 100 s for a $M_L = 4.0$ event. The second group includes earthquakes with a peak

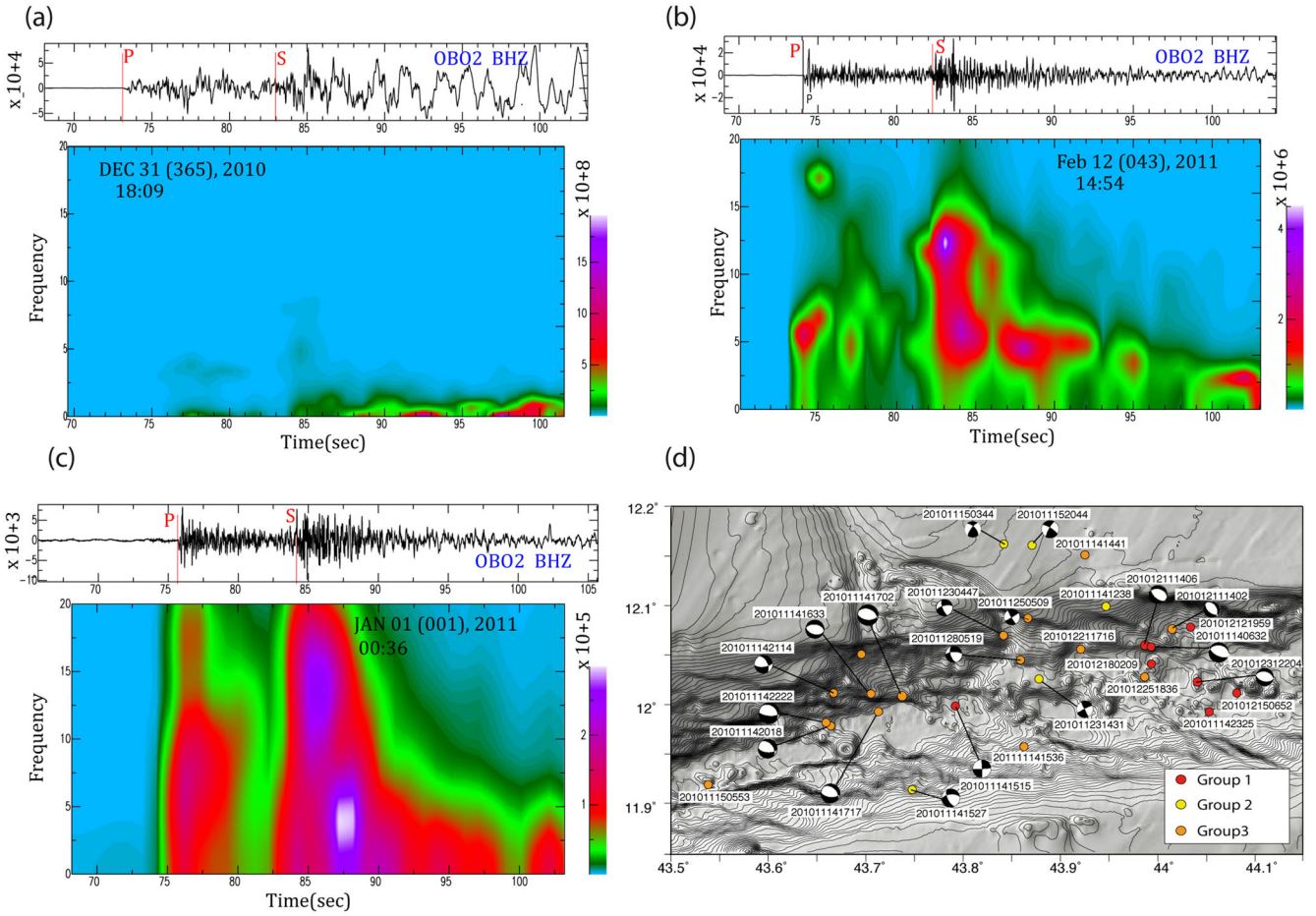

Figure 6. Examples of seismogram and spectrogram for the vertical channel recorded at the three-component Djiboutian station OBO2 for each three groups: (a) low-frequency earthquake, (b) high-frequency earthquake and (c) high- and low-frequency earthquake. Seismograms and spectrograms of the same events are represented on Aux_Mat-2 (Supporting Information), for the stations RSAR, ATA2 and GHAR. (d) Map of the locations and mechanisms of the earthquakes with a magnitude above 5. The colour scale indicates the group to which the event belongs as a function of its frequency content (see the text for description of each group).

in their spectra above 3 Hz (Fig. 6b). It is important to note that for a similar range of magnitude, the events of this group have a shorter duration than those of the first group. Together with some energy picks at frequency below 4 Hz, most of seismic energy is released in the frequency band of 4–10 Hz with a dominant frequency at ∼6–7 Hz. The third group corresponds to events with a mix of high and LF contents (Fig. 6c).

Looking only at the earthquakes with magnitude above 5.0 (Fig. 6d), it is notable that the epicentral locations of the events belonging to each of these three groups are not randomly distributed within the active area. With the exception of one earthquake, the LF earthquakes of the first group are clearly located within segment J, where the volcanism and magmatism is concentrated. With a lower magnitude, the LF event shown in Fig. 6(a) that occurred on 31 December 2010 (18:09 UTC) is located near the volcanic cones bounding the middle of the central graben from the southwest (E043.995°E, N12.013°), at a depth of ∼4.8 km. The events of the second group with high-frequency content are mainly located along the SW–NE-trending zone crossing the ridge valley, where the focal mechanisms are consistent with clear strike-slip or normal slip. The high-frequency event of 2011 February 12 (14:54 UTC) shown in Fig. 6(b) is located on the fan 2 (E043.896°, N12.056°) in the transfer zone between the central and western domains, at a depth of ∼5.1 km. Finally, the western domain where the events are mainly located within the ridge valley is characterized by earthquakes with a content of a combination of low and high frequencies.

5 TIME EVOLUTION OF THE SEISMIC EPISODE

5.1 Seismic moment release

The total cumulative seismic moment released during the monitoring period is ∼4.46 × 10^{18} Nm (Fig. 7a). Two thirds of this energy was released the first month following the onset of the swarm and one third during the following four months, from December 2010 to March 2011 (Fig. 7a). The large magnitude events largely contribute to this high value of seismic energy till the end of 2010. From the beginning of 2011, the number of earthquakes remains relatively high but few large magnitude earthquakes are recorded leading to a subdued seismic moment release. The cumulative seismic moment estimated for the main active area, segment J, in the central domain, is ∼2.76 × 10^{18} Nm, which accounts for ∼61.8 per cent of the total seismic moment release (Fig. 7a). The seismic cluster located 30 km southwest of the main swarm area (western domain) is characterized by strong events that account for 19 per cent of the

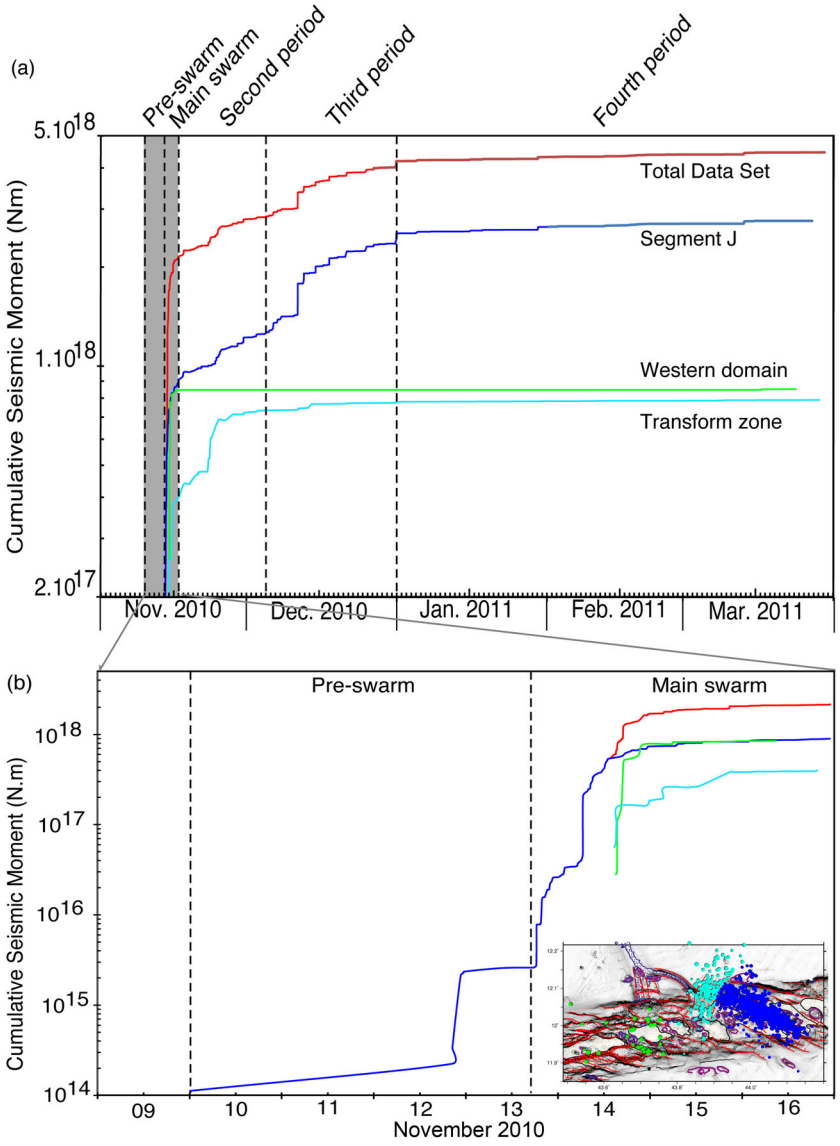

Figure 7. Time evolution of the cumulative seismic moment and the cumulative number of events (a) for the whole period under study and (b) for the first week at the onset of the episode. The insert at the bottom right corner of the graph (b) shows the location of each of the subsets considered in the calculation.

seismic energy with a cumulative seismic moment of 0.85×10^{18} Nm (Fig. 7). The seismic activity in the transform zone between the central and western domains is characterized by moderate seismic activity accounting for 17.7 per cent (0.79×10^{18} Nm) of the seismically released energy (Fig. 7). Other small clusters located to the east and the west of the main swarm area release 1.5 per cent of the total seismic energy.

Looking at the time evolution of both the cumulative seismic moment and the number of events (Fig. 7a), we distinguish several main time periods of distinct character, that we describe in the following, in order to better understand the evolution of this seismovolcanic episode.

5.2 Space–time evolution of seismicity over the episode

5.2.1 Pre-swarm

From November 10 to 13, 09:23 UTC, the first signs of activity in the area correspond to seven small and moderate earthquakes ($3.2 \leq M_L \leq 4.1$) accounting for very little of the seismic energy ($\sim 2.6 \times 10^{15}$ Nm). Five of them form an alignment along the 4 km long N105°E-trending fault at the NW end of the segment J central graben. Two of them occurred below the edge of the northern wall of the axial valley at the NW end of the segment J (Fig. 8a).

5.2.2 Main swarm

The first and main swarm started with an acceleration of the event occurrence from November 13 (17:35 UTC). A total of 166 events were recorded till November 17 (02:02 UTC), accounting for more than the half of the total seismic energy of the whole episode. We decompose the main swarm into three distinct time spans based on the seismicity evolution and the particular patterns drawn by the hypocentres.

First, during the five initial hours of the main swarm, on 2010 November 13, from 17:35 UTC to the end of the day, the seismic activity corresponds to 29 earthquakes mainly located along a

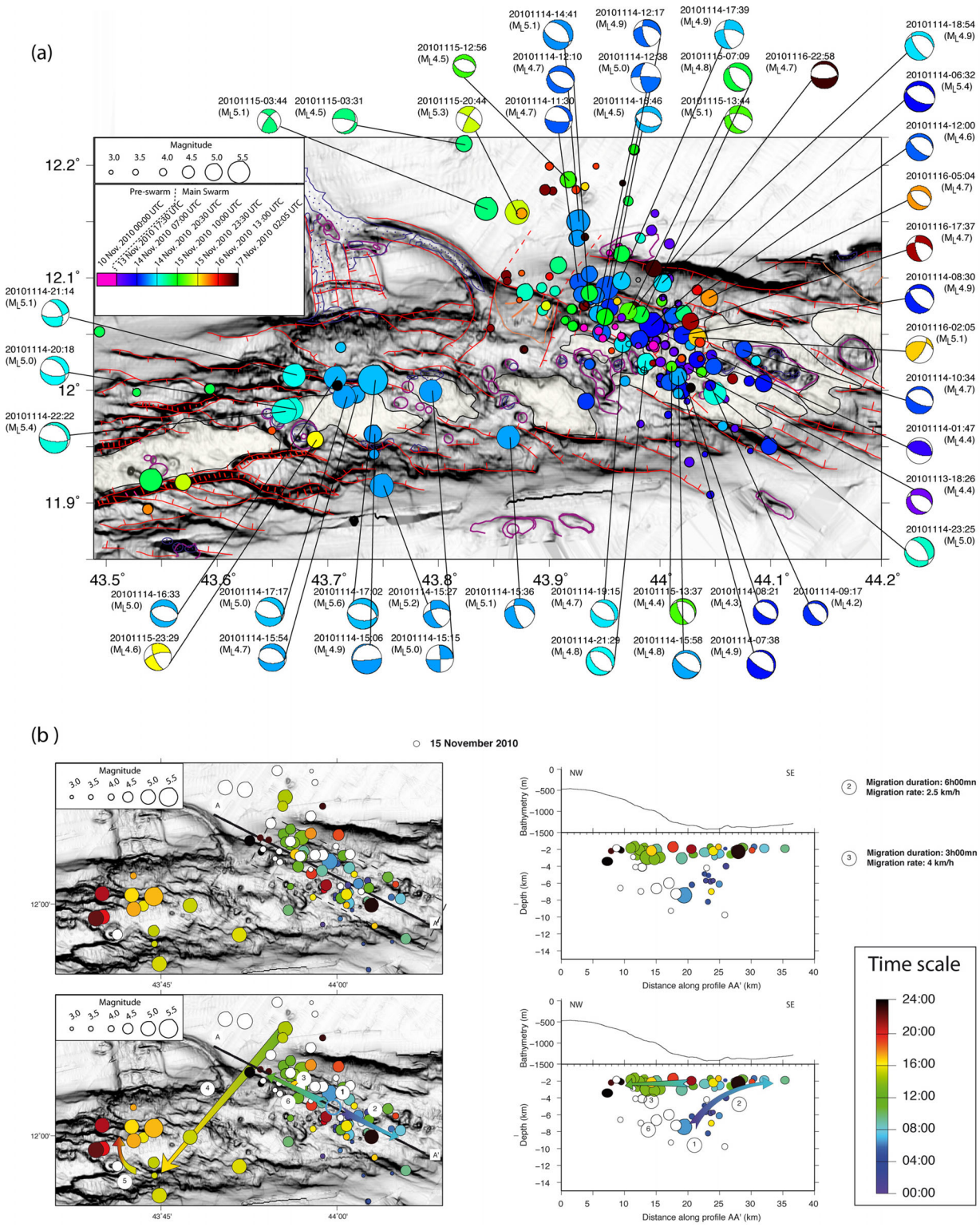

Figure 8. (a) Space–time evolution of the seismic activity during the pre-swarm (2010 November 10–13 09:23 UTC, pink colour) and during the main swarm (2010 November 13 17:35 UTC to 2010 November 17 02:05 UTC) with focal mechanism. (b) Space–time evolution of the seismic activity on 2010 November 14 on map and on the along-axis cross-section of segment J. Events with magnitude above 5.0 are indicated by thicker contours. The light blue circle indicates a circular aseismic gap surrounding a volcano at the NW end of the central graben.

NS-trending axis at E044° longitude (purple epicentres on Fig. 8a) and accounting for 0.02×10^{18} Nm. The maximum magnitude is 4.4, corresponding to an event (18:26 UTC) located at the centre of the inner floor of segment J, with a focal mechanism consistent with a normal slip along a SE-trending plane parallel to the bounding structures of the central graben (Fig. 8a).

Second, the seismic activity on November 14 is characterized by a combination of small and moderate events (Fig. 8b). The events

recorded during the six first hours are mostly low magnitude ($3.2 \leq M_L \leq 4.2$, 0.01×10^{18} Nm) and are concentrated below the centre of the segment J around 6 km depth. Except for one $M_L = 4.4$ event (01:47 UTC) located near the northern border of the central graben and characterized by reverse faulting along a SE-trending plane, all the focal mechanisms reveal normal faulting and encompass a nodal plane with the direction ranging from N115°E to N140°E. This trend is consistent with the evolution of direction of the bounding faults of the central graben from the NE to the SW (Fig. 8a). It is important to note that the area active during this period at the centre of the segment J reveals a circular aseismic gap surrounding a volcano at the NW end of the central graben during the following periods (Fig. 8b). From 06:05 UTC to the end of the day, the earthquake magnitude increases significantly, since it is above 4.2 for the 59 located events, and above 5.0 for 13 of them and a corresponding seismic moment reaching 1.7×10^{18} Nm. The largest event ($M_L =$ 5.4 at 06:32 UTC) is located at the mid-segment, at the foot of the slope of the northern ridge wall (Fig. 8b). The events that immediately follow between 6:00 and 09:30 UTC migrate SE-wards along the inner floor of the SE section of the segment J. It is interesting to note that all the focal mechanisms related with this time span are consistent with normal faulting including a high-dip plan (>80°). From 10:00 to 13:00 UTC, the events migrate northwestwards along the inner floor of the NW section of the segment J. The majority of the focal mechanisms show normal faulting, except for two events with strike-slip mechanisms along ~EW-trending nodal plane that occurred near the intersection of the northern end of segment J with the northern wall E–W-orientated at this level of the ridge (Fig. 8a).

Following the significant activity within the segment J graben, the events recorded after 14:41 UTC are characterized by high magnitude events (13 events with $M_L > 5.0$). They occurred first at the NW end of the segment J, below the northern margin of the rift valley and reached the transform zone between the central and the western domains. From 15:06 UTC on November 14, the activity shifted in the western domain and affected mainly the segments M and L (Fig. 8). Twenty events occurred in the area between segments L and O, with 18 of them with $M_L \geq 4.0$, including 8 with $M_L \geq 5.0$. This cluster started on November 14 in the western area includes the event with the largest magnitude in our catalogue ($M_L = 5.6$), which occurred at 17:02 UTC. Both normal faulting and pure strike-slip types of focal mechanisms are determined. However, the majority of them encompasses an EW-striking plan, in agreement with the EW-striking faults identified from the bathymetry data and bounding the rift valley and forming the ridge wall. Events located along or near the southern ridge wall of the western domain exhibit a general trend of E–W-trending normal faulting with a considerable strike-slip component (Fig. 8a). However, It is important to note that this area remains inactive over the following months, till March 2011, when another cluster of events affected this area (Fourth period).

Finally, during the two following days, the occurrence rate of events significantly decreases with ~30 events d^{-1}. The activity on November 15 is characterized by a swarm mainly located below the northwestern section of the segment J and the northern margin of the rift valley. The magnitudes remain high, with 3 events with magnitude above 5.0. The focal mechanisms are again consistent with a combination of strike-slip and normal faulting type. We note as well the occurrence of a moderate event ($M_L = 4.6$) along the volcanic chain separating the segments N and M, with a strike-slip fault mechanisms. On November 16, no large magnitude events were recorded, but the activity remained high, mainly concentrated at the centre of the segment J. Very few focal mechanisms have been determined. We note however the reverse-type mechanism, consistent with a NE-striking slipping plane.

5.2.3 *Second period*

Daily event distribution of the period November 17 (20:45 UTC) to December 4 shows that the seismic activity occurs by clusters interrupted by quiet periods and accompanied only by four events with $M_L \geq 5.0$. The seismic energy released during this period is low (0.7×10^{18} Nm) in comparison with the previous one. Fig. 9(a) shows that the activity is characterized by two swarms aligned along two orthogonal trends NW–SE and NE–SW. West of the longitude E043.9°, the earthquakes tend to align between two NE–SW parallel lines with a mean trend of N026°E. We note a 9 km long N157°E line extending from the mouth of the western canyon channel to the NW end of the segment K (Figs 3b and 9a). Two large events with $M_L = 5.0$ and 5.2 occurred at the NW end and near the SE end of this line, respectively. These two events are characterized by strike-slip mechanisms with a nodal plane trend of N158.5°E and N153°E, parallel to the trend of seismicity and the normal faults bounding the canyon channel (Fig. 9a). The seismic activity aligned along the NW–SE direction was confined to the NW end of segment J. Events with dominant normal faulting mechanisms occur at the centre of the segment. However, events with normal faulting mechanisms including an important strike-slip component and one E–W-trending nodal plane occur along the faults bounding the segment from the north and northeast. One event located at the base of the northern ridge wall exhibits a reverse faulting mechanism (Fig. 9a).

5.2.4 *Third period*

From December 5 to the end of 2010, we located 314 events with reduced location uncertainty due to the configuration of the network, which encompasses more stations on the Yemeni coast to the north of the active area (Aux_Mat-1 in the Supporting Information, Fig. 2). This period of time is characterized by the highest activity with many small events at the centre of segment J partly due to the lower detection threshold related to the optimal configuration of our network from 2010 December 15. Also, at least 13 moderate to strong events occurred on the northern and southern edges of the segment, with eight of them of magnitude $M_L \geq 5.0$, four with $M_L = 4.9$ and one with $M_L = 4.8$. The total seismic energy released is 1.4×10^{18} Nm. All the mechanisms of the events located on the northern edge of the segment are characterized by normal faulting with a nodal plane trend from N110°E to N125°E, except one event which is located near the volcanic highs bordering the central graben from the east and exhibits a strike-slip mechanism with an EW-trend plane (Fig. 9b). The events located on the southern edge of segment J are characterized by normal faulting with a small strike-slip component along planes with a direction between N130°E and N150°E (Fig. 9b). Some seismic activity aligned along the NE–SW direction at the western end of segment J is noticeable and 60 per cent of the events are clustered near the NW end of the central graben. Most of the shallow seismic activity (depth <4 km) was confined below the area situated between the volcanic cones at the segment centre and NW end of the central graben, with a seismic gap below the volcanic cones. Whereas there is no seismic activity in the western domain in December, two clusters occurred east of segment J. The first cluster corresponds to three events whose

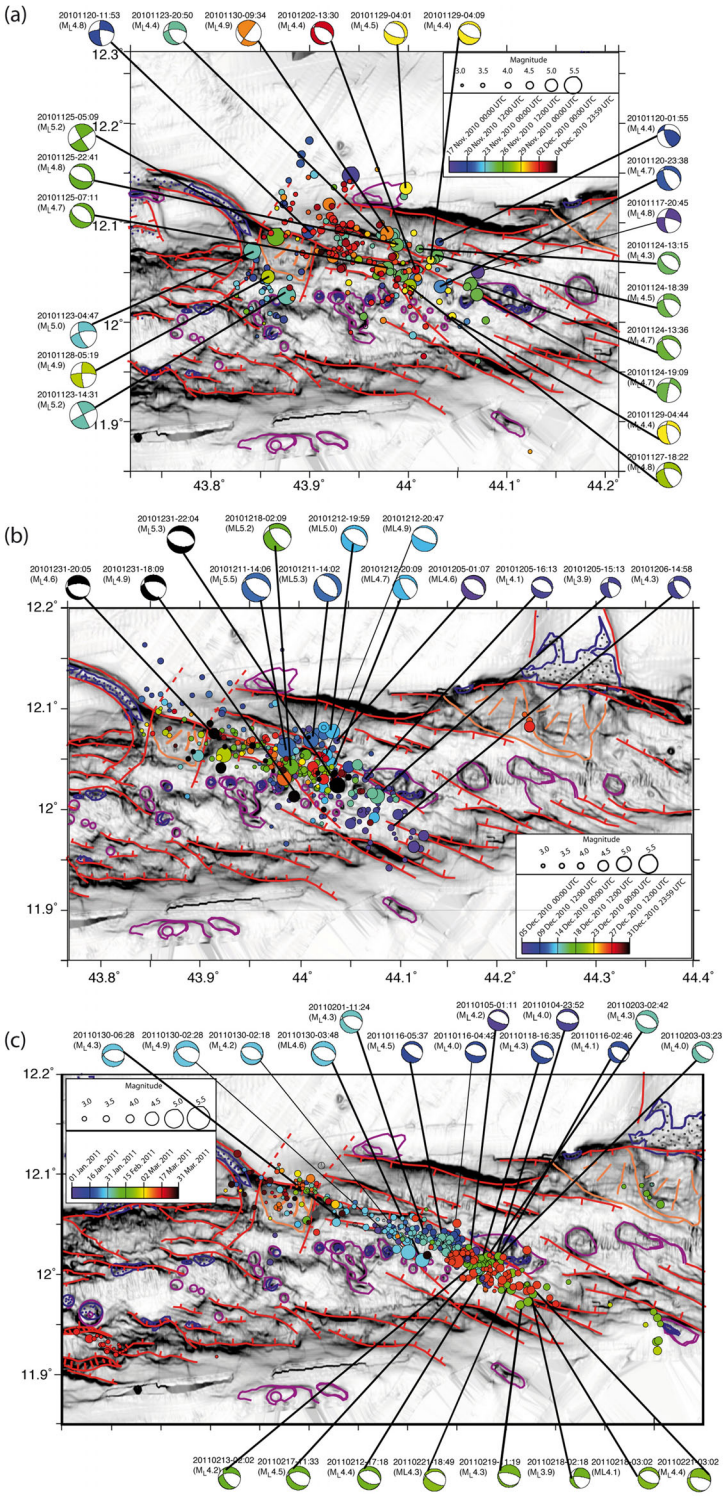

Figure 9. Space–time evolution of the seismic activity (a) during the second period (2010 November 17 20:45 UTC to 2010 December 4), (b) during the third period (2010 December 5 to 2010 December 31) and (c) during the fourth period (2011 January 1 to March 31).

hypocentres lie at a depth between 3.5 and 7 km and are aligned along the fault that divides fan 1 into two parts (Figs 3 and 4a). The second cluster consists of 14 events located at a volcanic complex area between the segments G and F with a depth ranging from 2 to 11 km (Figs 3 and 4a).

5.2.5 Fourth period

The fourth period corresponds to the regular activity during the months of January to March 2011. A total of 411 events were recorded during this period accounting for a very low cumulative seismic moment ($\sim 0.27 \times 10^{18}$ Nm). The highest magnitude

recorded is 4.9 on January 30 (02:28 UTC). An average of 4 events d^{-1} were recorded during this period, but the seismic activity is better described by a series of burst of activity on January (5,16,18,30), February (3,12,19) and March (13,15), 2011. We locate 157 earthquakes in January 2011, and the area of the main activity remained in the same location as in December. Most of the events occurred in the middle of the graben and are aligned along the bounding faults, in particular the faults that run along the NE–N–NW side of the graben as shown in Fig. 9(c). We note some concentrations of events at the location of the volcanic cones near the middle and NW end of the central graben. In addition, some small activity along the NE–SW trend to the NW of the graben and two events were located near segment G at the eastern end of the central domain. Most of the moderate size events ($M_L = 4.0$–4.9) are located in the central graben accompanied by normal faulting mechanisms with nodal planes parallel to the SE–NW trend (N100°E - N140°E) which is in agreement with the structures in the area (Fig. 9c).

The seismic activity during February and March 2011 has been clustered in seven distinct groups: the main seismic activity in the graben, a swarm centred on fan 2, and five small swarms to the east and west of the activity area (Figs 3a and 9c). Moreover, the slow migration of the seismic events is well represented by the seismic activity along the central graben in February. The event migration starts near the volcanic cone (location of the swarm onset) which is located near the NW end of the central graben and slowly moves southeastwards along the graben. This slow migration is accompanied by strong events with a normal faulting mechanism at the SE end of the graben at the vicinity of the base of the southern axial valley wall. This migration ends beyond this point by reaching an area located at shallow depth (<3 km) below the top edge of the wall at (044.253°E, 11.923°N). Eleven of the 21 moderate size events are located at the SE end of the segment, where eight of them are characterized by normal faulting along SE-trending planes (Fig. 9c). Two of the events are located near the volcanic highs bounding the central graben from the east and characterized by strike-slip mechanism with a small normal component with one EW-trending nodal plane (Fig. 9c). One of the events is located below the southern wall of the ridge and is characterized by a normal faulting mechanism with a strike-slip component.

The seismic activity in March is accompanied by small size events concentrated on fan 2 near the western channel and the SE end of the central graben. While the activity on fan 2 occurred at a small rate of 1–7 events d^{-1}, the seismic activity at the SE end is characterized by a strong burst of events on March 13 (Fig. 9c).

From 23:54 UTC March 15 to 00:39 UTC March 24, a swarm of 17 earthquakes at a depth ranging from 6.2 to 10.5 km is located at the base of the southern wall of the axial valley near segment N in the western domain. This swarm is characterized by small to moderate magnitude ($2.5 \leq M_L \leq 4.2$) events distributed within a narrow, 6 km long, N115°E-trending zone. Another swarm of 12 earthquakes occurred to the west from March 23 to March 26 near segment P. The small to moderate magnitude events of this swarm ($2.1 \leq M_L \leq 4.0$) occurred at a depth ranging from 10.8 to 16.9 km. To the east, we observe some activity in the same locations that the seismicity recorded in December near fan 1 and segment G.

5.2.6 Bursts of activity

The activity recorded over the whole episode is characterized by several bursts of activity presented by Fig. 10. A striking feature shared by most of these bursts is that the associated epicentres are located within segment J, but also define an alignment parallel to the segment axis. These bursts last for a few hours, except for the first main burst on November 14, which continued on the following day. This latter one is particularly interesting, and especially the chronology of the hypocentre distribution as described above (Fig. 8).

All the others bursts are smaller in terms of number of events, duration and size of the affected area. Each time, the released energy is between $\sim 4.1 \times 10^{15}$ Nm and $\sim 4.6 \times 10^{16}$ Nm, corresponding to one event with a magnitude between 4.4 and 5.1, respectively. Two kinds of bursts can be identified. First the bursts of events concentrated at the centre of the segment J (2011 January 16 and 30) for which most of the hypocentres are deep (>4 km). Second, the bursts of events spread from the segment centre and its ends (3 and 5 December, 13 March) and where most of the hypocentres are shallow (<3 km, see Fig. 10). For the three bursts affecting both the centre and the ends of the segment J, significant lateral migration is unclear due to the uncertainties on the locations of the small events. However, at the scale of the segment, we do observe that the first events of each burst are located at the centre whereas the later events are located far from the centre. This would correspond to a migration rate ranging from 0.5 to 5 km h^{-1}.

6 DISCUSSION

Together with high-resolution bathymetric data (Audin 1999), our detailed analysis of the seismicity during the November 2010–March 2011 episode in the Aden Gulf allows the clear identification of the activated structures belonging either to the ridge walls or the central valley. Both the space–time evolution and the characteristics of the seismicity confirm (1) the occurrence of volcanic activity at the centre of the ridge valley suggested by *in situ* measurements, and reveal (2) the occurrence of dike intrusions associated with a rifting episode, (3) the opening dynamics affecting one individual segment and (4) the interaction between the opening spreading segment J and the complex nascent transform zone.

6.1 Volcanic activity

Using a regional seismic network, it is difficult to interpret that underwater seismic activity is related to magmatic activity, that is, volcanic eruption and/or (a) magma intrusion(s), without any clear *in situ* field observations such as identification of fresh lava flows, bathymetric or morphological differences (e.g. Fox *et al.* 1992; Edwards *et al.* 2001). In our case, several observations suggest that this seismic episode corresponds to a significant magmatic activity, with probable lava flows over the sea floor within the ridge valley.

Our analysis of the space–time distribution of the earthquakes with respect to the main morphotectonic features within the active segment J reveals the role of the volcanic centres on the dynamics of this seismic event. In the case of D-MH segment activity in the Afar Depression, a ~4 to 10 km deep magma chamber is inferred from transient surface displacements in a very local area during the inter-diking periods, which are interpreted as movements of ascending magma replenishing the central reservoir located slightly south of the main volcanic chain marking the topography (Grandin *et al.* 2010). The lack of earthquakes would result from specific thermal conditions due to a focused zone of melt supply and/or the inadequate seismic network for the detection of small-magnitude events. Along segment J of the western Aden Ridge, two types of gaps of seismicity are distinguishable: the small circular areas

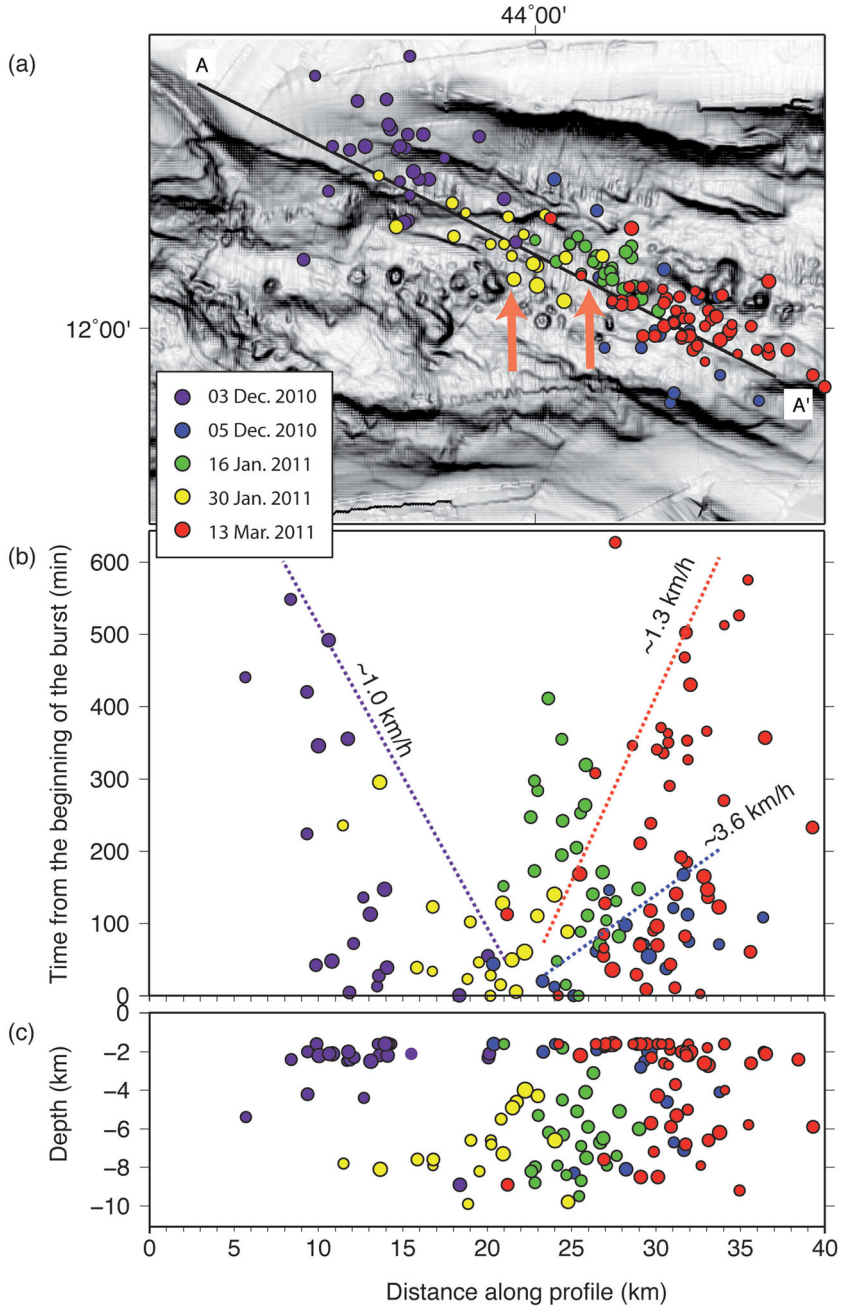

Figure 10. Space–time evolution of the seismic activity during the main bursts of activity (a) on the map, (b) on an along-axis time cross-section and (c) on an along-axis depth cross-section of segment J.

below the identifiable volcanic cones, and the large NW-dipping 1.5 km thick area (Fig. 4). Keeping in mind the larger uncertainties on the focal depth, in the same vertical columns of the small gaps, we see mostly moderate-magnitude deep events (located between 4 km and 12 km depth) and superficial small-magnitude events (located above 4 km) (see Fig. 4b for example). At the beginning of several peaks of activity, and particularly for the November 14, December 5 and January 30, several events occur at depth, below the seismic gap located underneath the central volcanic cone (Figs 8 and 10), providing probable evidence for the vertical ascent from deeper levels through a 'pipe', as observed in tomography images at the centre of oceanic segments (e.g. Canales *et al*. 2000; Madge *et al*. 2000; Dunn *et al*. 2005), either from a deep crustal magma chamber as inferred below the Krafla volcanic centre (Tryggvason 1986) or from a melting zone in the mantle. The large concentration of small magnitude and shallow earthquakes, particularly for the burst of January 16, could reveal faulting activity above the crustal magma reservoir, such as caldera faults or nearby faulting. This activity is associated with pressure changes into the reservoir, as it was shown during the inter-rifting period in the Asal-Ghoubbet rift in Djibouti, 20 yr after the 1978 Ardoukoba diking episode (Doubre *et al*. 2007a,b).

(1) ***The low-frequency events.*** The LF earthquakes, also called long-period or volcanic hybrid earthquakes have been the subject of many studies since they are commonly associated with magmatic activity and/or volcanic eruptions (Malone *et al*. 1983; Chouet *et al*.

1994; Lahr *et al*. 1994; Harrington & Brodsky 2007). The physical explanation of such events is still a key question and is usually attributed to the physical properties of the source material (liquid magma, hydrothermal fluids or gases) which generate LF signals during its movements (e.g. Aki & Koyanagi 1981; Chouet 1988; Leet 1991; Chouet 1996) or resonance of fluid-filled structure (Aki *et al*. 1977; Chouet 1985). In addition to the source, the LF content of the volcanic earthquakes is strongly dependent on the path effects (Harrington & Brodsky 2007; Cesca *et al*. 2008). LF signals from hybrid earthquakes have been observed and recorded over long durations across long distances during the 2009 earthquake swarm in Harrat-Lunayyir Saudi Arabia and are interpreted to be due to a dike intrusion (Pallister *et al*. 2010). In Afar, both types have been reported during the September 2005 D-MH magmatic events (Cote *et al*. 2010) and long period events have been observed at Kilauea Volcano in Hawaii (Cesca *et al*. 2008). LF earthquakes are observed in Icelandic volcanic regions, which are mostly due to magmatic intrusions or extrusions (Brandsdöttir & Einarsson 1992). In the western Aden ridge, the spatial distribution of the three groups of earthquakes based on their frequency content indicates that the LF events are located within segment J where volcanic cones are distinguishable in the bathymetry. The first large earthquake recorded on November 14 and located at depth below the main volcanic area is of very LF. Since we previously associated the occurrence of such earthquakes with the ascent of magma towards the shallow reservoir, they may result from the vibration of the magma conduits.

(2) ***The frequency–magnitude distribution.*** The frequency–magnitude distribution of the earthquakes recorded during the November 2010 episode shows high *b*-values, reaching 1.41 for the earthquakes located within segment J (Aux_Mat-5, Supporting Information). Such high *b*-values are usually found in volcanic and hydrothermal areas, where the occurrence of low-magnitude earthquakes is high and large events do not occur. We find a *b*-value of 1.20 for the rest of data, confirming that the seismic activity along the segment J is specific (Aux_Mat-5, Supporting Information). Taking into account that Hoffstetter & Beyth (2003) estimate a *b*-value of 1.05 for the period 1960–2000 in the Gulf of Aden, from Djibouti to E046°, this confirms that volcanic activity is temporally restricted to our period of study. We note that the Saudi rifting event was associated with a *b*-value of 1.20 (Pallister *et al*. 2010), however except for the surface deformation pattern deduced from InSAR and consistent with a dike opening, the volcanic activity is not clearly confirmed. The high *b*-value is also indicative of the evolved nature of the spreading area, since an increase in *b*-value is generally observed from continental to oceanic rifts. For example, *b*-values have been reported to increase from 1.0 in Tanzania and Kenya, to 1.06 and 1.13 in Afar and the Main Ethiopian rifts respectively (Kebede & Kulhànek 1994; Hoffstetter & Beyth 2003; Keir *et al*. 2006).

(3) ***In situ observations.*** Finally, constraints provided by a global communications company running sea bottom cables in the Gulf of Aden report multiple cable breakages in the region of our seismic swarms one year after the period of our study, between January and March 2012. Taking into account the melting temperature of 1084 °C for the copper, used as a protection components of the cable, the very high temperatures in this area strongly suggest that volcanic or intense hydrothermal activity occurred. The wire did not show sign of lava residue. This *in situ* information is very important, since it indicates that the volcanic episode affecting segment J lasted at least 15 months, whereas the seismic activity recorded by both Djiboutian and Yemenite seismic observatories remained moderate and regular in time (the Arta Geophysical Observatory recorded more than 300 earthquakes in the area from April 2011 to December 2011 with 19 events with magnitude above 4.0, Observatory staff, private communication).

6.2 New diking event

By comparing our results with the seismic results acquired during previous seismovolcanic episodes in subaerial rift zones, for which both geodetic (e.g. Abdallah *et al*. 1979; Wright *et al*. 2006; Grandin *et al*. 2009, 2012) and field constraints exist (e.g. Le Dain *et al*. 1979; Rowland *et al*. 2007), we infer that the seismic swarm in segment J of the western Gulf of Aden has nearly all the characteristics of seismic swarms related to diking episodes. This seismic activity and previous episodes share specific particularities described in the following, from which we attempt to determinate some quantitative characteristics.

(1) ***Peaks of activity.*** The evolution of the seismicity associated with rifting episodes is organized temporally by episodic peaks in activity, lasting from a few hours to a few days (Belachew *et al*. 2011; Grandin *et al*. 2011). During both the Ethiopian D-MH and the Icelandic Krafla sequences the peaks of activity have always been associated with individual diking events confirmed by geodetic measurements (e.g. Grandin *et al*. 2011). Between these peaks of activity, the duration of quiescent period ranges from one month to one year (see Wright 2012 and references therein). Ascending movement of magma to replenish the crustal magma chamber between dike injections occurred during the inter-diking periods (Grandin *et al*. 2010). During the five months of monitoring of the 2010 Aden episode, in addition to the main first swarm, we identify several small peaks associated with epicentres aligned along the rift axis (Fig. 10). Most of the hypocentres are concentrated within the three first kilometres of the sea floor, and could therefore correspond to dike intrusions. However, the time span between them ranges from one day to ∼one month. If these seismic peaks are all dike-induced, then the implication is that the necessary time to fill the magma chamber is very short, suggesting either a small-size reservoir or a significant magma supply from the mantle. If these peaks are not dike-induced then the main faults are seismically slipping at shallow depth responding to the regional tectonic stresses.

(2) ***Magnitude.*** Most of the seismovolcanic episodes associated with dike intrusions are characterized by a seismic sequence starting with earthquake(s), whose magnitude ranges from 5.0 to 5.5. In western Aden, ten events of magnitude above 5.0 occurred along segment J. In the case of the D-MH episode, 15 large events ($5.0 \leq M \leq 5.5$) were recorded during the first mega-dike intrusion in September 2005 (Ayele *et al*. 2007) and at least 25 in the following month (Ayele *et al*. 2009). Among the starting series, one of them ($M = 5.2$) was recorded in the same half-hour as the explosive eruption near the Dabbahu edifice, which might indicate, the volcanic origin of the event (Ayele *et al*. 2006). In the case of the 1978 Asal diking episode, the two main shocks ($M \geq 5.0$) were located in the sea, in the Ghoubbet Gulf corresponding to the rift zone of the segment, across which the maxima in extensional deformation was measured (Ruegg *et al*. 1979). This range of magnitude is typical of the sea floor spreading seismicity (Sykes 1970; Solomon *et al*. 1988) and reveals the thin brittle crustal layer along the oceanic ridge. As mentioned above, the occurrence of the first large event ($M = 5.4$, 2010 November 14 06:32 UTC) located below the main volcanic centre, at a depth of 7.5 km, therefore seems to be associated with the dynamics, and probably the replenishment

of the inferred underlying magma reservoir. The other events with magnitude above 5.0 are along the inner floor of segment J or in the vicinity of normal faults, suggesting that these events are associated with dike-induced faulting. Looking at the space–time decomposition of the activity, we first consider that the events recorded on 2010 November 14 and only located within segment J (see limits on Fig. 9a) are associated with the first intrusion. The total seismic moment release of this first series is $\sim 7.2 \times 10^{17}$ Nm, equivalent to an event of magnitude $M_w = 5.9$ (Hanks & Kanamori 1979). Adding the events of the subsequent three days, the total seismic moment reaches 9.1×10^{17} Nm. The seismic moment of the following peaks in activity do not exceed 4.6×10^{16} Nm.

The increased number of monitored dike intrusions allowed Nobile *et al*. (2012) to examine the associated seismic moment/geodetic moment ratio (SM/GM) at a range of rift stages. With the exception of the Dallol intrusion in northern Afar (Nobile *et al*. 2012), this ratio does not exceed 4 per cent in incipient oceanic rift segments of Afar and reaches values of 35.0 in continental context (Calais *et al*. 2008; Pallister *et al*. 2010). Following this trend, we infer a SM/GM ratio between 1.0 and 5.0 per cent for the oceanic episode in segment J in western Aden. Since the first intrusion during November 14–17 is associated with a seismic moment release of 9.1×10^{17} Nm, this results in a geodetic moment in the range of 1.82 to 9.1×10^{19} Nm. We followed the approach of Shuler & Nettles (2012) to estimate 0.58–2.9 m of horizontal opening by normal faulting based on a relation of Solomon *et al*. (1988) which links the moment to the dimensions and geometry of the rupture. This is consistent with the lack of fringes in the interferograms built from ALOS-PALSAR data on land, on the southern Yemenite coasts. From simple direct elastic modelling of opening crack at a depth between 0 and 10 km, the width of the main intrusion below the segment J associated with the main swarm does not exceed 5.0 m.

(3) ***Along-axis alignment of seismicity.*** The epicentres located at the vicinity of the segment J draw a very clear alignment perpendicular to the extension direction and concentrate within an ∼8 km wide band parallel to the rift zone (Brandsdöttir & Einarsson 1979; Keir *et al*. 2009; Belachew *et al*. 2011; Grandin *et al*. 2011). During the dike sequence of D-MH, each intrusion following the September 2005 intrusion is associated with individual earthquakes swarms with a length of 10–13 km, and a width of 2–4 km, corresponding to the width of axial faults triggered by each intrusion (Grandin *et al*. 2011). From different studies in D-MH, the length of the seismically active band broadly corresponds to the length of the subsiding zone revealed by the deformation field deduced from InSAR studies and field observations (Wright *et al*. 2006; Rowland *et al*. 2007; Grandin *et al*. 2009). In addition, the seismic cluster length approximates the length of the intrusion at depth. In the Gulf of Aden episode, the total length of the N115°-trending earthquake clusters along segment J is 40 km, and therefore suggests a similar length subsurface intrusion extending from the northern margin to the foot of the southern ridge wall. The first swarm corresponds to intrusions below both the northwestern and southeastern halves of segment J, while each of the following peaks occur in one direction. This pattern is similar to the intrusion sequence at D-MH, with the first mega dike intruded below both halves of the segment, with the following intrusions shorter and affecting one half of the rift. This pattern has been interpreted as the result of a high state of stress and/or a highly pressurized magma reservoir at the beginning of the sequence that induces the breaking of the crust along the whole segment length (Grandin *et al*. 2010). The following intrusions occur more or less in the same along-axis sections of the segment, suggesting that the deficit of opening is not fully filled after each of them. Also, we note that for most of the bursts the locations are next to the inferred crustal magma source below the main volcanic centre, which is consistent with a larger density of intrusions observed near the crustal magma reservoir along eroded volcanotectonic segments (Speight *et al*. 1982) and this confirms the role of the central crustal magma reservoir on the location of the highest magmatic dilatation.

From the comparisons of the displacement fields deduced from InSAR and field data in studies of the D-MH diking sequence, the width of the seismic band is indicative of the width of the subsiding zone and encompasses all the normal faults activated during the sequence and identified by the field observations (Rowland *et al*. 2007). Following the results of the InSAR inversions (Wright *et al*. 2006; Grandin *et al*. 2009, 2010; Hamling *et al*. 2009), the width of the seismically active band is wider than the opening width of the intrusion at depth, and underlines the dike-induced activity on normal faults located above the crack tip (Rubin & Pollard 1988). In our case, the 8 km wide alignment of the earthquakes along segment J suggests that the bounding normal faults already identified in the bathymetric data at segment J are activated in response to the intrusion, and that the construction of the topography of the segment probably results from a long-term repetition of dike intrusions along the segment axis. We note that the seismic band is clearly centred at the segment axis, suggesting that the 2010–2011 intrusions took place at the centre of the rift zone with no offset with respect to the topography. This contrasts the 2005 mega-dike in D-MH which was offset to the east of the rift axis (Grandin *et al*. 2009). Following Rubin & Pollard (1988) and assuming 65°-dipping normal faults, the maximum in opening is approximately at 8 km depth. The activated area narrows after December 15 (Figs 8b and c), which could be the result of the evolution of the network configuration. Alternatively, this could also reveal the asymmetry of the along-axis crustal structure, with more superficial intrusions reflecting a thinner brittle crust in the southern half of the segment as can be inferred from the asymmetry of the bathymetry.

(4) ***Hypocentral distribution and relation with volcanic centres.*** We observe that the seismogenic layer extends from the seafloor to ∼12 km. The occurrence of small magnitude earthquakes at shallow depth suggests that the state of stress in the crust is high and that the dikes intrude at shallower levels because of the brittle crust is thin. Along segment J, 42 per cent of the events are less shallow than 3 km. In general, deep earthquakes occurred at the beginning of bursts. This is interpreted previously as a quick replenishment of the magma reservoir before the intrusion implying that the time residence into the shallow magma chamber is short since the magma transits in a few hours from the deep level to the magma chamber and to eventually intrude into the rift zone of the segment. This magma transfer of a few hours is much faster than the transfers of a few months in other volcanic areas (e.g. Peltier *et al*. 2009; Druitt *et al*. 2012). Recharging of the magma chamber just before the intrusion could explain a part of the discrepancy between the volume of magma intruded in the rift zone and the deflation volume of the magma chamber modelled as a Mogi source from geodetic data (e.g. Wright *et al*. 2006; Grandin *et al*. 2009; Nobile *et al*. 2012).

(5) ***Migration of seismicity.*** The primary evidence for dike propagation is the migration of seismicity away from the main volcanic centre towards the segment ends. Magma likely propagates into dikes following a process of hydraulic fracturing with the central crustal reservoir being the main pressure source (e.g. Gudmundsson

1998; Doubre & Geoffroy 2003). The deceleration of the seismic migration is consistent with a decrease in pressure within the reservoir coeval with the magma withdrawal. The migration rate of the seismicity in the western Gulf of Aden is 1–4 km h^{-1}, which is comparable to the migration rates reported for D-MH where typical velocities were 0.54–5.4 km h^{-1} range (Ayele *et al*. 2009; Keir *et al*. 2009; Belachew *et al*. 2011). Our rates are higher than the 0.36–1.8 km h^{-1} reported for Krafla-Iceland (Einarsson & Brandsdöttir 1980). We also note that after the intrusion reaches its final length, we observe the occurrence of small events along the dike (Fig. 10). This pattern is similar to what was observed in D-MH (Keir *et al*. 2009; Belachew *et al*. 2011; Grandin *et al*. 2011) and interpreted as earthquakes resulting from the inflation of the dike or by the thermal stresses near the dike walls.

6.3 Activity along one individual segment and magma intrusion as the main extension process

At this longitude, the structure of the Aden Ridge is characterized by left-stepping en-echelon segments which overlap by more than ∼20 km, corresponding to ∼80 per cent of their length. Nevertheless, the seismic activity during the five months following the sequence of November 2010 is confined within one individual segment. Such rifting episodes are usually seen as transient displacement accommodating the far field plate motion along the plate boundary. The total seismic moment for segment J during the five months under study is to $\sim 2.76 \times 10^{18}$ Nm (Fig. 7), from which we estimate a geodetic moment of ∼5.5 to 27.6×10^{19} Nm, and magnitudes of horizontal opening of 1.76–8.8 m along the whole segment. This amount of opening is equivalent to ∼135–677 yr of spreading at this part of the ridge where the spreading rate is 1.3 cm yr^{-1}. The structure of the ridge axis with en-echelon segments overlapping over 80 per cent of their length, implies that if there is a deficit of opening along the divergent plate boundary, the concentration of extensional stresses along the ridge due to the far field plate motion is distributed over several overlapping en-echelon segments. The activity during the 2010–2011 episode occurring in one segment only and with adjacent segment quiescent provides evidence that the release of the stresses is controlled by the discrete supply of magma into the plumbing magma system of individual segments (Madge *et al*. 2000). Therefore, this observation shows that the dynamics of an oceanic spreading segment is independent from the adjacent segments. In addition, our work shows that the magma system feeding the crustal reservoir(s) of one segment is probably isolated from similar systems below other segments, even when adjacent segment overlap a significant distance. Further, this strongly supports a models by which the dynamics of a divergent plate boundary is controlled by the presence of a series of punctuated mantle sources connected independently to the shallow magma reservoirs of the segments.

6.4 Nascent transform zone

The seismic activity and focal mechanisms help constrain the interaction between rift opening and transform faulting. Near canyon 2, we note that several events with a strike-slip focal mechanism show both senses of horizontal slip along parallel planes. Oceanic transform faults are found along all spreading ridges except at along ultra-slow and ultra-fast settings. According to recent reviews (Choi *et al*. 2008; Gerya 2012), their origin remains unclear. Transform faults can nucleate spontaneously in accreting and cooling plate of wax as demonstrated by old analogue models (e.g. Freund & Merzer 1979). Analogue models of the oblique rifting specific to the Gulf of Aden evidence that such rift segmentation is structured by numerous transfer and transform zones. Block rotations cause steep shear in the rift centre. The steep faults are roughly parallel to the opening direction and well oriented to become potentially transform faults (Autin *et al*. 2010b).

The first group of strike-slip focal mechanisms include an E–W-trending focal plan, which is consistent with the dextral faults evidence in the bathymetry data and reported by previous studies done in the area (e.g. Audin 1999; Dauteuil *et al*. 2001). The focal mechanisms of earthquakes, mainly located along the northern end of segment J and on the southern shoulder of segment M, also show horizontal slip along the EW-trending planes. Such EW-trending faults are visible in the bathymetry, and their formation could be attributed to the E–W component of the regional stress due to oblique extension. The second group of focal mechanisms encompass one nodal plane mostly parallel to the ∼N40°E-trending relative motion of the Arabia and Somalia plates. The earthquakes belonging to this group are located at the western end of the active segment J near the mouth of canyon 2 and draw an alignment perpendicular to the direction of the axis of the segments and parallel to the regional maximum tensile stress. These earthquakes result in right-lateral strike-slip motion along ∼N039° ± 8°E-striking faults planes that we interpret as an incipient transform fault between two ridge segments. This nascent transform is located where a change in ridge-axis trend occurred (Fig. 1b). Following previous studies, the transform area is the part located between 43.91°E and the location where recent lava flows are observed east of 44.20°E (Dauteuil *et al*. 2001; Hébert *et al*. 2001). However, the transform part is the area located between the two NNW–SSE trending normal faults at the locus of the two canyons cutting the northern shoulder of the axial valley. This area is the westernmost part of the E-W trending axial valley where well-developed en-echelon N115°E-trending basins exist. West of this area, the trend of the axial valley is N075°E with deep basins covered by a thick layer of interrupted deposits and the en-echelon structures built on the southern ridge wall (Choukroune *et al*. 1988), but not at the main valley.

The earthquakes belonging to third group of strike-slip mechanisms (N065°E ± 8°/N155°E ± 8°) occur at the vicinity of the faults bounding the canyons, and especially along the western one (canyon 2, Fig. 3c). Near this latter canyon, tectonic structures are parallel to the ∼N150°–155°E direction, which corresponds to the direction of one of the nodal planes of the focal mechanisms, suggesting that left-lateral strike-slip faulting may occur along these planes (Figs 4c and 8c). It is not clear to which stress regime such movement could be attributed. Choukroune *et al*. (1988) proposed a model of N145°E-striking rifts for the Gulf of Tadjura based on CYADEN dives results. Lépine & Hirn (1992) described left-lateral strike-slip motion on N150°E-trending faults, resulting in clockwise rotations of the blocks between the faults (Fig. 1b). Manighetti *et al*. (1997) proposed two different kinematic models to explain the successive attempts of the Gulf of Aden ridge to propagate through Bab-El Mandeb strait resulting in the construction of the two canyons and bounding structures (Fig. 1). Their finite kinematic model extends from 5 to 0.7 Ma and explains a relative motion between Arabia-Somalia (1.73 cm yr^{-1} parallel to N039°E direction), Arabia-Danakil (0.7 cm yr^{-1} along N65°E) and Somalia-Danakil of 1.2 cm yr^{-1} along N025°E direction. From these models, no clear mechanism could explain the eastward displacement of the fan 2 from the mouth of canyon 2. Our results which show both left-lateral and right-lateral motion at the same location and on distinct

orientations may explain the displacement of fan-deposits 2 together with the curvature of the two canyon channels (Fig. 3a). Combining observations and results, we propose that this area is a transfer zone between the E–W and N75E-oriented ridges and corresponds to the western boundary of the transform zone between true oceanic lithosphere in the east and a transitional lithosphere in the west.

7 CONCLUSIONS

By combining data from permanent and temporary networks in Djibouti and Yemen, we obtained accurate locations of the earthquakes associated with the large seismic episode started on November 2010 in the western Gulf of Aden. From precise location process, the analysis of the space–time distribution of the magnitude 2.1–5.6 events, their source mechanisms and their frequency content, we are able to distinguish several seismic swarms related to distinct tectonic features. A large part of seismicity is concentrated along an active spreading segment, and the characteristics of this seismicity share numerous similitudes with recent dike intrusions monitored along subaerial segments. The dynamics of this opening segment confirms the mechanisms and processes involved during an active rifting episode, in particular the crucial role of the magmatic system. The seismicity struck only one segment of a highly oblique, en-echelon and overlapping system, and suggests the independence of the magma plumbing systems below each discrete ridge segment.

Finally, the opening dynamics of the segment induces movement along oblique planes related to a transfer zone, that we interpret as a nascent transform zone. This transform zone corresponds to the western limit of the 'true' oceanic lithosphere in the Gulf before the transitional or continental lithosphere of Afar in the vicinity of the Gulf of Tadjura. Therefore, this episode demonstrates the close interaction between the active rifting and/or spreading processes and the development of the transform faults in the oceanic lithosphere. Our results may suggest that transform fault onset and evolution may be controlled by the opening of the segment and more precisely follow the focus magma supply on one segment. At the scale of the structure of a spreading ridge, the magmatic plumbing system could trigger the initiation of a transform zone.

ACKNOWLEDGEMENTS

The instruments temporary deployed in Djibouti and Yemen belong to the French national pool of portable seismic instruments Sismob-RESIF, the IUEM-UBO and EOST-IPGS temporary seismic networks. This work was supported by the following projects funded by the French National Agency (ANR, France): ANR-YOCMAL, ANR-DoRA and Rift2ridge, CNRS-INSU-PICS Yemen, GSMRB Yemen and Actions Marges. We thank the French Embassy in Sana'a (J.G. Sarkis, J. Dechezlepretre and C. Bousquet) and the French army in Djibouti for logistical support during the installation of the networks. This work could not have been done without the precious collaboration with OGA and CERD in Djibouti (OGA), SVOC and GSMRB in Yemen. We are grateful to Encarnation, and Regis Coquelin de Lisle, the local governors and the people of the Yemen governorates for their help during the field work. Our deep thoughts go to our colleague Kassim Mohamed, now deceased, and his family. We gratefully acknowledge the information provided to us regarding the damage to submarine cables in the Gulf of Aden during 2011. Due to reasons of confidentiality we are unable to release details of the company or individuals that provided us with the information. DK is supported by NERC grant NE/L013932/1.

REFERENCES

Abdallah, A. *et al.*, 1979. Relevance of Afar seismicity and volcanism to the mechanics of accreting plate boundaries, *Nature,* **282,** 17–23.

Ahmed, A. *et al.*, 2013. Crustal structure of the rifted volcanic margins and uplifted plateau of Western Yemen from receiver function analysis, *Geophys. J. Int.,* **193,** 1673–1690.

Ahmed, A. *et al.*, 2014. Crustal structure of the Gulf of Aden southern margin: evidence from receiver functions on Socotra Island (Yemen), *Tectonophysics,* **637,** 251–267.

Aki, K. & Koyanagi, R., 1981. Deep volcanic tremor and magma ascent mechanism under Kilauea, Hawaii, *J. geophys. Res.,* **86**(B8), 7095–7109.

Aki, K., Fehler, M. & Das, S., 1977. Source mechanisms of volcanic tremor: fluid-driven crack models and their application to the 1963 Kilauea eruption, *J. Volcanol. Geotherm. Res.,* **2,** 259–287.

Al-Amri, A.M., Fnais, M.S., Abdel-Rahman, K., Mogren, S. & Al-Dabbagh, M., 2012. Geochronological dating and stratigraphic sequences of Harrat Lunayyir, NW Saudi Arabia, *Int. J. Phys. Sci.,* **7**(20), 2791–2805.

Al-Zahrani, H.A., Fnais, M.S., Al-Amri, A.M. & Abdel-Rahman, K., 2012. Tectonic framework of Lunayyir area, northwest Saudi Arabia through aftershock sequence analysis of 19 May, 2009 earthquake and aeromagnetic data, *Int. J. Phys. Sci.,* **7**(44), 5821–5833.

Audin, L., 1999. Penetration de la dorsal d'Aden dans la depression Afar entre 20 et 4 Ma, *PhD Thesis,* University de Paris 7 et Institute de Physique du Globe de Paris, Paris, 278 p.

Autin, J. *et al.*, 2010a. Continental break-up history of a deep magma-poor margin from seismic reflection data (northeastern Gulf of Aden margin, offshore Oman), *Geophys. J. Int.,* **180,** 501–519.

Autin, J., Bellahsen, N., Husson, L., Beslier, M.O., Leroy, S. & d'Acremont, E., 2010b. Analogue models of oblique rifting in a cold lithosphere, *Tectonics,* **29,** TC 6016, doi:10.1029/2010TC002671.

Ayele, A., Nyblade, A.A., Langston, C.A., Cara, M. & Leveque, J.-J., 2006. New evidence for Afro-Arabian plate separation in south Afar, in *The Afar Volcanic Province in the East African Rift System,* pp. 133–141, Vol. 256, eds Yirgu, G., Ebinger, C.J. & Maguire, P.K.H., Geological Society (Special Publications).

Ayele, A. *et al.*, 2007. The volcano-seismic crisis in Afar, Ethiopia, starting September 2005, *Earth planet. Sci. Lett.,* **255**(1–2), 177–187.

Ayele, A. *et al.*, 2009. September 2005 mega-dike emplacement in the Manda-Harraro nascent oceanic rift (Afar depression), *Geophys. Res. Lett.,* **36,** L20306, doi:10.1029/2009GL039605.

Baer, G. & Hamiel, Y., 2010. Form and growth of an embryonic continental rift: InSAR observations and modelling of the 2009 western Arabia rifting episode, *Geophys. J. Int.,* **182,** 155–167.

Barberi, F., Civetta, L. & Varet, J., 1980. Sr isotopic composition of Afar volcanics and its implication for mantle evolution, *Earth planet. Sci. Lett.,* **50,** 247–259.

Belachew, M., Ebinger, C., Coté, D., Keir, D., Rowland, J.V., Hammond, J.O.S. & Ayele, A., 2011. Comparison of dike intrusions in an incipient seafloor-spreading segment in Afar, Ethiopia: seismicity perspectives, *J. geophys. Res.,* **116,** B06405, doi:10.1029/2010JB007908.

Bellahsen, N. *et al.*, 2013. Pre-existing oblique transfer zones and transfer/transform relationships in continental margins: new insights from the southeastern Gulf of Aden, Socotra Island, Yemen, *Tectonophysics,* **607,** 32–50.

Blackman, D., Nishimura, C. & Orcutt, J., 2000. Seismoacoustic recordings of a spreading episode on the Mohns Ridge, *J. geophys. Res.,* **105**(B5), doi:10.1029/2000JB900011.

Brandsdöttir, B. & Einarsson, P., 1979. Seismic activity associated with the September 1977 deflation of Krafla volcano in north-eastern Iceland, *J. Volcanol. Geotherm. Res.,* **6,** 197–212.

Brandsdöttir, B. & Einarsson, P., 1992. Volcanic tremor and low-frequency earthquakes in Iceland, in *Volcanic Seismology,* pp. 212–222, eds Gasparini, P., Scarpa, R. & Aki, K., Springer.

Calais, E. *et al.*, 2008. Strain accommodation by slow slip and diking in a youthful continental rift, East Africa, *Nature,* **456,** 783–787.

Canales, J.P., Collins, J.A., Escartin, J. & Detrick, R.S., 2000. Seismic structure across the rift valley of the Mid-Atlantic ridge at 23°20′N (MARK area): implications for crustal accretion processes at slow spreading ridges, *J. geophys. Res.,* **105**(B12), 28 411–28 425.

Cannat, M., 1996. How thick is the magmatic crust at slow spreading oceanic ridges?, *J. geophys. Res.,* **101**(B2), doi:10.1029/95JB03116.

Cesca, S., Battaglia, J., Dahm, T., Tessmer, E., Heimann, S. & Okubo, P., 2008. Effects of topography and crustal heterogeneities on the source estimation of LP event at Kilauea volcano, *Geophys. J. Int.,* **172,** 1219–1236.

Choi, E., Lavier, L. & Gurnis, M., 2008. Thermomechanics of mid-ocean ridge segmentation, *Phys. Earth planet. Inter.,* **171,** 374–386.

Chouet, B., 1985. Excitation of a buried magmatic pipe: a seismic source model for volcanic tremor, *J. geophys. Res.,* **90,** 1881–1893.

Chouet, B., 1988. Resonance of a fluid-driven crack: radiation properties and implications for the source of long-period events and harmonic tremor, *J. geophys. Res.,* **93,** 4375–4400.

Chouet, B.A., 1996. Long-period volcano seismicity: its source and use in eruption forecasting, *Nature,* **380,** 309–316.

Chouet, B.A., Page, R.A., Stephens, C.D., Lahr, J.C. & Power, J.A., 1994. Precursory swarms of long-period events at Redoubt Volcano (1989–1990), Alaska: their origin and use as a forecasting tool, *J. Volcanol. Geotherm. Res.,* **62,** 95–135.

Choukroune, P., Francheteau, J., Auvray, l.B., Auzende, J.M., Brun, J.P., Sichler, B., Arthaud, F. & Lepine, J.C., 1988. Tectonics of an incipient oceanic rift, *Mar. Geophys. Res.,* **9,** 147–163.

Corbeau, J. *et al.*, 2014. Uppermost mantle velocity from Pn tomography in the Gulf of Aden, *Geosphere,* **10**(5), 958–968.

Cote, M.D., Belachew, M., Quillen, A.C., Ebinger, C.J., Keir, D., Ayele, A. & Wright, T., 2010. Low-frequency hybrid earthquakes near a magma chamber in afar: quantifying path effects, *Bull. seism. Soc. Am.,* **100**(5A), 1892–1903.

Courtillot, V., Galdeano, A. & Le Mouel, J.P., 1980. Propagation of an accreting plate boundary: a discussion of new aeromagnetic data in the Gulf of Tadjurah and Southern Afar, *Earth planet. Sci. Lett.,* **47,** 144–160.

d'Acremont, E., Leroy, S., Maia, M., Patriat, P., Beslier, M.O., Bellahsen, N., Fournier, M. & Gente, P., 2006. Structure and evolution of the eastern Gulf of Aden: insights from magnetic and gravity data (Encens-Sheba/MD117 cruise), *Geophys. J. Int.,* **165,** 786–803.

d'Acremont, E., Leroy, S., Maia, M., Gente, P. & Autin, J., 2010. Volcanism, jump and propagation on the Sheba ridge, eastern Gulf of Aden: segmentation evolution and implications for oceanic accretion processes, *Geophys. J. Int.,* **180,** 535–551.

Dauteuil, O., Huchon, P., Quemeneur, F. & Souriot, T., 2001. Propagation of an oblique spreading centre: the western Gulf of Aden, *Tectonophysics,* **332,** 423–442.

DeMets, C., Gordon, R.G. & Argus, D.F., 2010. Geologically current plate motions, *Geophys. J. Int.,* **181,** 1–80.

Doubre, C. & Geoffroy, L., 2003. Rift-zone development around a plume-related magma centre on the Isle of Skye (Scotland): a model for stress inversions, *Terra Nova,* **15,** 230–237.

Doubre, C., Manighetti, I., Dorbath, C., Dorbath, L., Jacques, E. & Delmond, J.-C., 2007a. Crustal structure and magmato-tectonic processes in an active rift (Asal-Ghoubbet, Afar, East Africa): 1. Insights from a 5-month seismological experiment, *J. geophys. Res.,* **112**(B11), B05405, doi:10.1029/2005JB003940.

Doubre, C., Manighetti, I., Dorbath, C., Dorbath, L., Bertil, D., Jacques, E. & Delmond, J.-C., 2007b. Crustal structure and magmato-tectonic processes in an active rift (Asal-Ghoubbet, Afar, East-Africa). Part 2: Insights from the 23 years recording of seismicity since the last rifting event, *J. geophys. Res.,* **112,** doi:10.1029/2006JB004333.

Doubre, C. *et al.*, 2009. Dynamics of rifting in two active rift segments in Afar—geodetic and structural studies—DoRA project, in *AGU Fall Meeting Abstracts,* Vol. 31, 1817 pp.

Dreger, D.S. & Helmberger, D.V., 1993. Determination of source parameters at regional distances with single station or sparse network data, *J. geophys. Res.,* **98,** 8107–8125.

Druitt, T.H., Costa, F., Deloule, E., Dungan, M. & Scaillet, B., 2012. Decadal to monthly timescales of magma transfer and reservoir growth at a caldera volcano, *Nature,* **482,** 77–80.

Dunn, R.A., Lekić, V., Detrick, R.S. & Toomey, D.R., 2005. Three-dimensional seismic structure of the Mid-Atlantic Ridge (35°N): evidence for focused melt supply and lower crustal dike injection, *J. geophys. Res.,* **110,** B09101, doi:10.1029/2004JB003473.

Dziak, R.P., Bohnenstiehl, D.R., Matsumoto, H., Fowler, M.J., Haxel, J.H., Tolstoy, M. & Waldhauser, M., 2009. The January 2006 seafloor spreading event at 9°50'N, East Pacific Rise: Ridge dike intrusion and transform fault interactions from regional hydroacoustic data, *Geochem. Geophys. Geosyst.,* **10,** Q06T06, doi:10.7916/D89S1P46.

Dziewonski, A.M., Chou, T.A. & Woodhouse, J.H., 1981. Determination of earthquake source parameters from waveform data for studies of global and regional seismicity, *J. geophys. Res.,* **86,** 2825–2852.

Ebinger, C.J. *et al.*, 2008. Capturing magma intrusion and faulting processes during continental rupture: seismicity of the Dabbahu (Afar) rift, *Geophys. J. Int.,* **174**(3), 1138–1152.

Ebinger, C.J., van Wijk, J. & Keir, D., 2013. The time scales of continental rifting: implications for global processes, *Geol. Soc. Am. Spec. Pap.,* **500,** 371–396.

Edwards, M.H., Kurras, G.J., Tolstoy, M., Bohnenstiehl, D.R., Coakley, B.J. & Cochran, J.R., 2001. Evidence of recent volcanic activity on the ultraslow-spreading Gakkel ridge, *Nature,* **409,** 808–812.

Egloff, F. *et al.*, 1991. Contrasting structural styles of the eastern and westernmargins of the southern Red Sea: the 1988 SONNE experiment, *Tectonophysics,* **198,** 329–353.

Einarsson, P. & Brandsdöttir, B., 1980. Seismological evidence for lateral magma intrusion during the July 1978 deflation of the Krafla volcano in NE-Iceland, *J. geophys. Res.,* **47,** 160–165.

Ferguson, D.J. *et al.*, 2013. Melting during late-stage rifting in Afar is hot and deep, *Nature,* **499**(7456), 70–73.

Field, L. *et al.*, 2012. Integrated field, satellite and petrological observations of the November 2010 eruption of Erta Ale, *Bull. Volcanol.,* **74**(10), 2251–2271.

Fournier, M., Patriat, P. & Leroy, S., 2001. Reappraisal of the Arabia-India-Somalia triple junction kinematics, *Earth planet. Sci. Lett.,* **189,** 103–114.

Fournier, M. *et al.*, 2010. Arabia-Somalia plate kinematics, evolution of the Aden-Owen-Carlsberg triple junction, and opening of the Gulf of Aden, *J. geophys. Res.,* **115,** B04102, doi:10.1029/2008JB006257.

Fox, C.G., Chadwick, W.W., Jr. & Embley, R.W., 1992. Detection of changes in ridge-crest morphology using repeated multibeam sonar surveys, *J. geophys. Res.,* **97**(B7), 11 149–11 162.

Fox, C.G., Radford, W.E., Dziak, R.P., Lau, T.-K., Matsumoto, H. & Schreiner, A.E., 1995. Acoustic detection of a seafloor spreading episode on the Juan de Fuca Ridge using military hydrophone arrays, *Geophys. Res. Lett.,* **22,** 131–134.

Freund, R. & Merzer, A.M., 1976. Anisotropic origin of transform faults, *Science,* **192,** 137–138.

Gerya, T., 2012. Origin and models of oceanic transform faults, *Tectonophysics,* **522–523,** 34–54.

Grandin, R. *et al.*, 2009. September 2005 Manda Hararo–Dabbahu rifting event, Afar (Ethiopia): constraints provided by geodetic data, *J. geophys. Res.,* **114,** B08404, doi:10.1029/2008JB005843.

Grandin, R., Socquet, A., Jacques, E., Mazzoni, N., de Chabalier, J.B. & King, G.C.P., 2010. Sequence of rifting in Afar, Manda-Hararo rift, Ethiopia, 2005–2009: time–space evolution and interactions between dikes from interferometric synthetic aperture radar and static stress change modeling, *J. geophys. Res.,* **115,** B10413, doi:10.1029/2009JB000815.

Grandin, R. *et al.*, 2011. Seismicity during lateral dike propagation: insights from new data in the recent Manda Hararo–Dabbahu rifting episode (Afar, Ethiopia), *Geochem. Geophys. Geosyst.,* **12,** Q04B08, doi:10.1029/2010GC003434.

Grandin, R., Socquet, A., Doubre, C., Jacques, E. & King, G.C.P., 2012. Elastic thickness control of lateral dike intrusion at mid-ocean ridges, *Earth planet. Sci. Lett.,* **319–320,** 83–95.

Gudmundsson, A., 1998. Magma chambers modeled as cavities explain the formation of rift zone central volcanoes and their eruption and intrusion statistics, *J. geophys. Res.,* **103**(B4), 7401–7412.

Hamling, I.J. *et al.*, 2009. Geodetic observations of the ongoing Dabbahu rifting episode: new dike intrusions in 2006 and 2007, *Geophys. J. Int.,* **178,** 989–1003.

Hamlyn, J.E. *et al.*, 2014. Seismicity and subsidence following the 2011 Nabro eruption, Eritrea: insights into the plumbing system of an off-rift volcano, *J. geophys. Res.,* doi:10.1002/2014JB011395.

Hanks, T.C. & Kanamori, H., 1979. A moment magnitude scale, *J. geophys. Res.,* **84,** 2348–2350.

Hansen, S. & Nyblade, A.A., 2013. The deep seismic structure of the Ethiopia/Afar hotspot and the African superplume, *Geophys. J. Int.,* **194**(1), 118–124.

Harrington, R.M. & Brodsky, E.E., 2007. Volcanic hybrid earthquakes that are brittle-failure events, *Geophys. Res. Lett.,* **34,** L06308, doi:10.1029/2006GL028714.

Hébert, H., Deplus, C., Huchon, P., Khanbari, K. & Audin, L., 2001. Lithospheric structure of a nascent spreading ridge inferred from gravity data: the western Gulf of Aden, *J. geophys. Res.,* **106,** 26 345–26 363.

Hjörleifsdottir, V. & Ekström, G., 2010. Effects of three-dimensional Earth structure on CMT earthquake parameters, *Phys. Earth planet. Inter.,* **179,** 178–190.

Hoffstetter, R. & Beyth, M., 2003. The Afar Depression: interpretation of the 1960–2000 earthquakes, *Geophys. J. Int.,* **155,** 715–732.

Huang, P. & Solomon, S., 1988. Centroid depths of mid-ocean ridge earthquakes: dependence on spreading rate, *J. geophys. Res.,* **93**(B11), doi:10.1029/88JB03224.

Kawakatsu, H., 1995. Automated near-realtime CMT inversion, *Geophys. Res. Lett.,* **22,** 2569–2572.

Kebede, F. & Kulhánek, O., 1994. Spatial and temporal variations of *b*-values along the East African rift system and the southern Red Sea, *Phys. Earth planet. Inter.,* **83,** 249–64.

Keir, D., Ebinger, C.J., Stuart, G.W., Daly, E. & Ayele, A., 2006. Strain accommodation by magmatism and faulting as rifting proceeds to breakup: seismicity of the northern Ethiopian rift, *J. geophys. Res.,* **111**(B5), doi:10.1029/2005JB003748.

Keir, D. *et al.*, 2009. Evidence for focused magmatic accretion at segment centers from lateral dike injections captured beneath the Red Sea rift in Afar, *Geology,* **37,** 59–62.

Keir, D., Pagli, C., Bastow, I.D. & Ayele, A., 2011. The magma-assisted removal of Arabia in Afar: evidence from dike injection in the Ethiopian rift captured using InSAR and seismicity, *Tectonics,* **30,** TC2008, doi:10.1029/2010TC002785.

Kikuchi, M. & Kanamori, H., 1991. Inversion of complex body waves-III, *Bull. seism. Soc. Am.,* **81,** 2335–2350.

Korostelev, F. *et al.*, 2014. Crustal and upper mantle structure beneath southwestern margin of the Arabian Peninsula from teleseismic tomography, *Geochem. Geophys. Geosyst.,* **15**(7), 2850–2864.

Lahr, J.C., Chouet, B.A., Stephens, C.D., Power, J.A. & Page, R.A., 1994. Earthquake classification, location, and error analysis in a volcanic environment: implications for the magmatic system of the 1989–1990 eruptions at Redoubt Volcano, Alaska, *J. Volcanol. Geotherm. Res.,* **62,** 137–151.

Laughton, A.S. & Tramontini, C., 1969. Recent studies of the crustal structure of the Gulf of Aden, *Tectonophysics,* **8,** 359–375.

Laughton, A.S., Whitmarsh, R.B. & Jones, M.T., 1970. The evolution of the Gulf of Aden, *Phil. Trans. R. Soc. Lond., A,* **267,** 227–266.

Le Dain, A.-Y., Robineau, B. & Tapponnier, P., 1979. Les effets tectoniques de l'événement sismique et magmatique de Novembre 1978 dans le rift d'Asal-Ghoubbet, *Bull. Soc. Géol. France,* **7**(6), 817–822.

Leet, R.C., 1991. Investigation of Hydrothermal Boiling and Steam Quenching as Possible Sources of Volcanic Tremor and Geothermal Ground Noise, *PhD thesis,* University of Washington, Final Report, DOE Grant No. DE-FG606-88ER13979.

Lépine, J.C. & Hirn, A., 1992. Seismotectonics in the Republic of Djibouti linking the Afar Depression and the Gulf of Aden, *Tectonophysics,* **209,** 65–86.

Leroy, S., d'Acremont, E., Tiberi, C., Basuyau, C., Autin, J., Lucazeau, F. & Sloan, H., 2010a. Recent off-axis volcanism in the eastern Gulf of Aden: implications for plume-ridge interaction, *Earth planet. Sci. Lett.,* **293,** 140–153.

Leroy, S. *et al.*, 2010b. Contrasted styles of rifting in the eastern Gulf of Aden: a combined wide-angle MCS and Heat flow survey, *Geochem. Geophys. Geosyst.,* **11,** 1–14.

Leroy, S. *et al.*, 2012. From rifting to oceanic spreading in the Gulf of Aden: a synthesis, *Arab J. Geosci.,* doi:10.1007/s12517-011-0475-4.

Lucazeau, F. *et al.*, 2009. Post-rift volcanism and high heat-flow at the ocean-continent transition of the eastern Gulf of Aden, *Terra Nova,* **21,** 285–292.

Madge, L.S., Barclay, A.H., Toomey, D.R., Detrick, R.S. & Collins, J.A., 2000. Crustal magma plumbing within a segment of the Mid-Atlantic Ridge, 35°N, *Earth planet. Sci. Lett.,* **175,** 55–67.

Makris, J. & Ginzburg, A., 1987. The Afar depression: transition between continental rifting and sea-floor spreading, *Tectonophysics,* **141,** 199–214.

Malone, S.D., Boyko, C. & Weaver, C.S., 1983. Seismic precursors to the mount st. Helens eruptions in 1981 and 1982, *Science,* **221**(4618), 1376–1378.

Manighetti, I., Tapponnier, P., Courtillot, V., Gruszow, S. & Gillot, P.Y., 1997. Propagation of rifting along the Arabia-Somalia Plate Boundary: The Gulfs of Aden and Tadjoura, *J. geophys. Res.,* **102**(B2), 2681–2710.

Mohr, P., 1987. Structural styles of continental rifting in Ethiopia: reverse decollements, EOS, *Trans. Am. geophys. Un.,* **68**(35), 721–730.

Nobile, A., Pagli, C., Keir, D., Wright, T.J., Ayele, A., Ruch, J. & Acocella, V., 2012. Dike-fault interaction during the 2004 Dallol intrusion at the northern edge of the Erta Ale Ridge (Afar, Ethiopia), *Geophys. Res. Lett.,* **39,** L19305, doi:10.1029/2012GL053152.

Ottemöller, L., Voss, P. & Havskov, J., 2011. *SEISAN Earthquake Analysis Software for Windows, Solaris, Linux and MacOSX,* version 9.1, Bergen University, Bergen, 368 p.

Pagli, C., Wright, T.J., Ebinger, C.J., Yun, S., Cann, J.R., Barnie, T. & Ayele, A., 2012. Shallow axial magma chamber at the slow-spreading Erta Ale Ridge, *Nat. Geosci.,* **5,** 284–288.

Pallister, J.S. *et al.*, 2010. Broad accommodation of rift-related extension recorded by dike intrusion in Saudi Arabia, *Nat. Geosci.,* **3,** 705–712.

Peltier, A., Bachelery, P. & Staudacher, T., 2009. Magma transport and storage at Piton de La Fournaise (La Réunion) between 1972 and 2007: a review of geophysical and geochemical data, *J. Volcanol. Geotherm. Res.,* **184,** 93–108.

Robinet, J., Razin, P., Serra-Kiel, J., Gallardo-Garcia, A., Leroy, S., Roger, J. & Grelaud, C., 2013. The Paleogene pre-rift to syn-rift succession in the Dhofar margin (northeastern Gulf of Aden): stratigraphy and depositional environments, *Tectonophysics,* **607,** 1–19.

Rooney, T., Herzberg, C. & Bastow, I., 2012. Elevated mantle temperature beneath East Africa, *Geology,* **40**(1), 27–30.

Rowland, J.V., Baker, E., Ebinger, C.J., Keir, D., Kidane, T., Biggs, J., Hayward, N. & Wright, T.J., 2007. Fault growth at a nascent slow-spreading ridge: 2005 Dabbahu rifting episode, Afar, *Geophys. J. Int.,* **171,** 1226–1246.

Rubin, A. & Pollard, D.D., 1988. Dike-induced faulting on rift zones of Iceland and Afar, *Geology,* **16,** 413–417.

Ruegg, J.C., 1975. Main results about the crustal and upper mantle structure of the Djibouti region (T.F.A.I), in *Afar Depression of Ethiopia,* pp. 120–134E, eds Pilger, A. & Rsler, A., Schweizerbart'sche Verlagsbuchhandlung.

Ruegg, J.C., Lepine, J.C. & Tarantola, A., 1979. Geodetic measurements associated with a seismo-volcanic crisis in Afar, *Geophys. Res. Lett.,* **6,** 817–820.

Shuler, A. & Nettles, M., 2012. Earthquake source parameters for the 2010 western Gulf of Aden rifting episode, *Geophys. J. Int.,* **199**(2), 1111–1122.

Sigurdsson, O., 1980. Surface deformation of the Krafla fissure swarm in two rifting events, *J. Geophys.,* **47,** 154–159.

Solomon, S.C., Huang, P.Y. & Meinke, L., 1988. The seismic moment budget of slowly spreading ridges, *Nature,* **334,** 58–60.

Speight, J., Skelhorn, R., Sloan, T. & Knaap, R., 1982. The dike swarms of Scotland, in *Igneous Rocks of the British Isles,* pp. 449–621, ed. Sutherland, D.S., Wiley.

Sykes, L.R., 1970. Earthquake swarms and sea-floor spreading, *J. geophys. Res.,* **75,** 6598–6611.

Tard, F., Masse, P., Walgenwitz, F. & Gruneisen, P., 1991. The volcanic passive margin in the visinity of Aden, Yemen, *Bull. Cent. Rech. Explor. Prod.,* **15,** 1–9.

Tolstoy, M., Bohnenstiehl, D.R. & Edwards, M.H., 2001. Seismic character of volcanic activity at the ultraslow-spreading Gakkel Ridge, *Geology,* **29**(12), 1139–1142.

Tolstoy, M., Diebold, J., Doermann, L., Nooner, S., Webb, S.C., Bohenstiehl, D.R., Crone, T.J. & Holmes, R.C., 2009. Broadband calibration of R/V Marcus G. Thompson four-string seismic sources, *Geochem. Geophys. Geosyst.,* **10,** Q08011, doi:10.1029/2009GC002451.

Toomey, D.R., Solomon, S.C., Purdy, G.M. & Murray, M.H., 1985. Microearthquakes beneath the Median Valley of the Mid-Atlantic Ridge near 23°N: hypocentres and focal mechanisms, *J. geophys. Res.,* **90,** 5443–5458.

Tryggvason, E., 1986. Multiple magma reservoirs in a rift zone volcano: ground deformation and magma transport during the September 1984 eruption of Krafla, Iceland, *J. Volcanol. Geotherm. Res.,* **28,** 1–44.

Vergne, J., Doubre, C., Mohamed, K., Tiberi, C., Leroy, S. & Maggi, A., 2010. Geometry of the Arabia-Somalia plate boundary into afar: preliminary results from the seismic profile across the Asal Rift (Djibouti), *Abstract T31C-2195,* AGU, San Francisco, CA.

Weidner, D.J. & Aki, K., 1973. Focal depth and mechanism of mid-ocean ridge earthquake, *J. geophys. Res.,* **78**(11), 1818–1831.

Wolfe, C.J., Purdy, G.M., Toomey, D.R. & Solomon, S.C., 1995. Microearthquake characteristics and crustal velocity structure at 29°N on the Mid-Atlantic Ridge: the architecture of a slow spreading segment, *J. geophys. Res.,* **100,** 24 449–24 472.

Wright, T.J., 2012. Geophysical constraints on the dynamics of spreading centres from rifting episodes on land, *Nat. Geosci.,* **5,** 242–250.

Wright, T.J., Ebinger, C., Biggs, J., Ayele, A., Yirgu, G.J., Keir, D. & Stork, A., 2006. Magma-maintained rift segmentation at continental rupture in the 2005 Afar diking episode, *Nature,* **442,** 291–294.

Yagi, Y., 2004. Moment Tensor inversion program, IISEE lecture notes, *Technical report,* Tsukuba, Japan.

SUPPORTING INFORMATION

Additional Supporting Information may be found in the online version of this paper:

Aux_Mat-1.

Aux_Mat-2. *P*-wave velocity – depth section showing different velocity structures derived from active seismic profiles carried out in different tectonic regions of the study area, including the velocity model used by the Djibouti seismic network, the Yemen seismic network (derived from Egloff *et al*. 1991), LT6235-6236 active seismic profiles western Gulf of Aden (Laughton & Tramontini 1969) and active seismic profiles in the northern and southern areas of Djibouti (Ruegg 1975). The intermediate velocity model used in this study is shown by red curve.

Aux_Mat-3. Comparison of the vertical and horizontal location errors before and after the evolution of the seismic network on December 15.

Aux_Mat-4. Linear relation between M_L and the log of the seismic moment for the 85 events for which we estimated the moment tensor. The linear fit is deduced by least squares minimization on the values of M_L ($R^2 = 0.6$).

Aux_Mat-5. Log cumulative number of earthquakes against local magnitude (M_L) plots for the whole episode and (b) for the segment J (dark blue events Fig. 7). Triangles show the cumulative earthquake frequency–magnitude (Gutemberg-Richter) distribution of earthquakes. The solid line shows best fit truncated GR function for both samples, with b the slope and a the intercept. 'a' is the total number of earthquakes above the magnitude of completeness (M_c) and 'b' is given by the formula $b = \log(10) / (\text{m\_average}—M_c)$; where m_average is the average local magnitude of the sample. The marked magnitude M_c ($M_L = 4$) is the magnitude of completeness, above which the catalogue is considered as complete.

Aux_Mat-6. Examples of seismogram and spectrogram for the vertical channel recorded at the three-component stations RSAR, ATA2 and GHAR for (a) low-frequency earthquake, (b) high-frequency earthquake and (c) high- and low-frequency earthquake.

(http://gji.oxfordjournals.org/lookup/suppl/doi:10.1093/gji/ggw068/-/DC1).